# Adaptation to cystine limitation stress promotes PDAC tumor growth and metastasis through translational upregulation of OxPPP

Yunzhan Li[1,*], Zekun Li[2,*], Dongxiao Sun[3], Bo Ni[2], Mingjun Tan[1], Ashley E. Shay[4], Min Wang[1], Chenyang Meng[2], , Guangcong Shen[2], Boyang Fu[2], Yueying Shan[2], Tianxin Zhou[2], Yongjie Xie[2], Kun-Ming Chen[5], Bin Qiao[6], Yunkun Dang[7], Scot R. Kimball[1], Pankaj K. Singh[8], Xiuchao Wang[2,#], Jihui Hao[2,#], Shengyu Yang[1,9,#]

[1] Department of Cellular and Molecular Physiology, Penn State Cancer Institute, Penn State College of Medicine, Hershey, PA 17033

[2] Department of Pancreatic Cancer, Tianjin Medical University Cancer Institute and Hospital, National Clinical Research Center for Cancer, Key Laboratory of Cancer Prevention and Therapy, Tianjin 300060, China.

[3] Department of Pharmacology, Penn State College of Medicine, Hershey, PA 17033

[4] Metabolomics Core Facility, The Pennsylvania State University, University Park, PA 16802

[5] Department of Biochemistry and Molecular Biology, Penn State Cancer Institute, Penn State College of Medicine, Hershey, PA 17033

[6] School of Chemical Engineering, Tianjin University, Tianjin 300072, China

[7] State Key Laboratory for Conservation and Utilization of Bio-Resource in Yunnan, Key Laboratory for Southwest Microbial Diversity of the Ministry of Education, Yunnan Key Laboratory of Cell Metabolism and Diseases, Center for Life Science, School of Life Sciences, Yunnan University, Kunming 650021, China.

[8] Department of Oncology Science, University of Oklahoma Health Sciences Center, Oklahoma City, Oklahoma.

[9] Requests for further information and resources should be directed to and will be fulfilled by the lead contact, Shengu Yang (sxy99@psu.edu).

* These authors contributed equally to this research article.

# To whom correspondence should be addressed:

Xiuchao Wang, Department of Pancreatic Cancer, Tianjin Medical University Cancer Institute and Hospital, Tianjin 300060, China. E-mail: wangxiuchao@tjmuch.com

Jihui Hao, Department of Pancreatic Cancer, Tianjin Medical University Cancer Institute and Hospital, Tianjin 300060, China. E-mail: haojihui@tjmuch.com

Shengyu Yang, Penn State College of Medicine, Department of Cellular and Molecular Physiology, MC H166, 500 University Dr., Hershey, PA 17033-0850. E-mail: sxy99@psu.edu

## Abstract

Cystine/cysteine is critical for antioxidant response and sulfur metabolism in cancer cells and is one of the most depleted amino acids in the PDAC microenvironment. The effects of cystine limitation stress (CLS) on PDAC progression are poorly understood. Here we report that adaptation to CLS (CLSA) promotes PDAC cell proliferation and tumor growth through translational upregulation of the oxidative pentose phosphate pathway (OxPPP). OxPPP activates the *de novo* synthesis of nucleotides and fatty acids to support tumor growth. Our data suggested that much like hypoxia, CLS in the tumor microenvironment could promote PDAC tumor growth and metastasis through upregulating anabolic metabolism of nucleotides and lipids.

## Introduction

Pancreatic ductal adenocarcinoma (PDAC) is a highly aggressive cancer with a 5-year survival rate of 13%. The PDAC tumor microenvironment is characteristically nutrient deprived due to desmoplasia, poor vascularization and hyperactive cancer metabolism[1,2]. The plasticity in cancer metabolism is critical for cancer cells to overcome nutrient limitation stress and to support tumor growth and progression [1]. However, the roles of nutrient limitation stress in PDAC tumor growth and progression remained incompletely understood.

Cystine ($Cys_2$) and cysteine (Cys) are important amino acid nutrients for the antioxidant response and sulfur metabolism[3,4]. In the oxidative blood circulation, Cys is oxidized into $Cys_2$. SLC7A11, the functional subunit of the $Cys_2$ / glutamate antiporter system $xc^-$, is responsible for cystine uptake[3,5]. In the cell $Cys_2$ is reduced to Cys and used for the synthesis of essential sulfur metabolites, such as glutathione (GSH) and iron-sulfur clusters (Fe-S)[6]. Although $Cys_2$ and Cys are non-essential amino acids, cancer cells depend on exogenous $Cys_2$ for antioxidant response and survival [4,7]. $Cys_2$ deprivation induces ferroptosis, a type of iron and lipid peroxidation-dependent cell death in pancreatic cancer and other cancer [7-12]. Intriguingly, $Cys_2$ and Cys are among the most depleted amino acids in the PDAC tissue and tumor interstitial fluid[13,14]. It is unclear how PDAC cells adapt to the chronic $Cys_2$ limitation stress (CLS) and how such adaptation affects PDAC tumor growth and progression.

Cancer cells upregulate anabolic metabolism such as *de novo* synthesis of nucleotides and fatty acids (FA) to support cancer cell proliferation and tumor growth[15]. The oxidative pentose phosphate pathway (OxPPP) provides ribose-5-phosphate (R5P) for the *de novo* synthesis of nucleotides[16] and the NADPH for antioxidant response and *de novo* FA synthesis [17,18]. G6PD (glucose-6-phosphate dehydrogenase), PGLS (6-phosphogluconolactonase) and PGD (phosphogluconate dehydrogenase) are the three enzymes in the OxPPP, which use G6P (glucose-6-phosphate) as precursor for the synthesis of R5P and the reduction of NADP+ to NADPH[16]. G6PD catalyzes the rate limiting step of OxPPP and is upregulated in many cancer types including PDAC [19].

While the upregulation of FA synthesis provides lipids to support membrane synthesis during cancer cell proliferation, the accumulation of excess FA could lead to lipotoxicity and cell damage[20-22]. To protect cells from lipotoxicity, excess FA is esterified by diacylglycerol O-acyltransferase 1 and 2 (DGAT1 and 2) into triacylglycerides (TG) and stored in the lipid droplets (LD) [22, 23]. LD accumulation correlates with tumor aggressiveness and therapy resistance in many cancer types[24]. In addition to serving as lipid storage organelles, LD are crucial for cell survival

under stress. Stresses such as ER stress, acidosis and chemotherapeutic agents can promote lipolysis and/or lipogenesis[23,25]. The storage of excess FA, polyunsaturated fatty acids, lipid peroxidation products and acyl-ceramides in LD allows cells to avoid stress-induced lipotoxicity and cell death[26]. There are recent reports indicating that DGAT1/2 inhibitors could be used to inhibit tumor growth and improve the efficacy of chemotherapy and radiotherapy in colorectal cancer, melanoma and glioblastoma [20,27]. However, the roles of LD in PDAC remain poorly understood[28].

Here we investigated the effects of chronic CLS in PDAC. We found that adaptation to CLS (CLSA) promotes PDAC cell proliferation, ferroptosis resistance and tumor growth. CLSA PDAC cells translationally upregulate OxPPP enzymes G6PD, PGD and / or PGLS to promote biosynthesis of NADPH, nucleotides and lipids..

## Results

### Adaptation to cystine limitation stress promotes PDAC cell proliferation, ferroptosis resistance and tumor growth.

To determine whether PDAC cells might be subjected to CLS, we determined the levels Cys and $Cys_2$ in PDAC and para-tumor normal pancreatic tumor tissue from C57BL/6 mice orthotopically implanted with a PDAC line derived from the KPC ($Kras^{LSL\text{-}G12D}$/$Trp53^{LSL\text{-}R172H}$/ Pdx1-Cre) model. The levels of Cys and $Cys_2$ in tumor tissues were approximately 90% (for Cys) to 50% (for $Cys_2$) lower when compared to para-tumor normal pancreatic tissues (Fig.1A). The Cys to $Cys_2$ ratios were higher in adjacent pancreas tissues than in tumors (Fig. 1A). Similarly, we observed a significant decrease in Cys levels in patient PDAC tissues when compared to para-tumor normal pancreas control in a cohort of 10 PDAC patients (Fig. 1B). These data suggest that PDAC cells are subjected to chronic CLS.

Most cell culture media (e.g. DMEM or RPMI) contain 200 μM $Cys_2$, which is significantly higher than $Cys_2$ levels in the human plasma (25-50 μM)[29]. Cells cultured *in vitro* have higher demand for $Cys_2$ due to direct exposure to ambient $O_2$. As shown in Fig. S1A, decreasing $Cys_2$ concentrations to 50 μM or lower in MiaPaCa-2 media led to increased phosphorylation of eIF2α and expression of ATF4, which suggested the activation of the integrated stress response by $Cys_2$ limitation. As expected, acute reduction of $Cys_2$ from 200 μM to 50 or 25 μM led to lipid peroxidation and ferroptosis-like cell death in PDAC cells in in 72 hours (Fig. S1B-S1D). Approximately 5 to 30 percent of PDAC cells were able to adapt to CLS at 25 μM and resume cell growth and proliferation after 3-4 weeks exposure to CLS (Fig. 1C and Fig. S1E). The proportion of PDAC cells adapted to 50 μM CLS were much higher (Fig. S1E). Here we use CLSA-25 and CLSA-50 to refer to PDAC cells adapted to 50 or 25 μM $Cys_2$, respectively. Culturing PDAC cells in medium containing 25 μM $Cys_2$ reduced the intracellular Cys levels by approximately 75% to 90% in 24-48 hours (Fig. 1D). Although Cys level modestly recovered in CLSA-25 MiaPaCa-2 and PANC-1 cells after 4-week adaptation, it was still ~60-50 % lower than in naïve control cells cultured in approximately 75% to 90% in 24-48 hours (Fig. 1D). Although Cys level modestly recovered in CLSA-25 MiaPaCa-2 and PANC-1 cells after 4-week adaptation, it was still ~60-50 % lower than in naïve control cells cultured in $Cys_2$ replete medium (Fig. 1D). No recovery of intracellular Cys was observed in CLSA-25 Pan02 and KPC cells (Fig. 1D). Interestingly, CLSA PDAC cells proliferate much faster than parental cells, despite severe reduction of intracellular Cys (Fig 1E). Given the considerable interest in using $Cys_2$ deprivation

agents as potential cancer therapeutics, we asked whether CLS induced by pharmacological agents might have similar effects on PDAC cells. We previously reported that imidazole ketone erastin (IKE) induced ferroptosis in PDAC cell lines and patient-derived organoids (PDOs) [30]. As shown in Fig. 1F-1G, PDAC organoids adapted to IKE-induced CLS (CLSA-I, for inhibitor induced adaptation) also grew faster than naïve control PDOs.

GPX4 is the sole glutathione peroxidase responsible for scavenging lipid peroxide and preventing ferroptosis. To determine the effect of CLSA on ferroptosis sensitivities, we treated CLSA PDAC cells or PDOs with GPX4 inhibitor RSL-3. As shown in Fig. 1H and 1I, the $IC_{50}$ of RSL-3 in CLSA-25 cells and CLSA-I PDOs increased dramatically by 10 to 500-fold when compared to naïve controls. CLSA-50 cells also developed ferroptosis resistance, although to a lesser extent (Fig. 1I).

To determine whether CLSA affects tumor growth, we implanted CLSA Pan02 and KPC cells and their naïve control orthotopically in the pancreas of C57BL/6 mice. Mice implanted with CLSA-50 Pan02 cells grew modestly larger tumors, with increased numbers of liver metastases when compared to the control group (Fig. 1J-1L). The liver metastasis incident increased from 30% in control to 90% in CLSA-50 group (Fig. 1K). In the KPC xenograft experiment, the growth of orthotopically implanted CLSA-25 KPC tumors were dramatically faster than control tumors, although no metastasis was detected in either group (Fig. 1N**)**. Similarly, orthotopically implanted CLSA-I PDOs developed larger tumors when compared to naïve control (Fig. 1O-1P). Taken together, our data showed that CLSA promotes PDAC cell proliferation, ferroptosis resistance and tumor growth.

To determine whether nutrient limitation of other amino acids might induce similar adaptation in PDAC cells, we cultured MiaPaCa-2 cells in medium containing reduced amounts of glutamine (400 μM), tryptophan (10 μM) or arginine (2 μM), respectively. These amino acids and concentrations were selected based on previous reports showing their depletion in PDAC[13,31] . MiaPaCa-2 cells were able to proliferate in Trp-limited media, but not in Glu- or Arg-limited conditions for 2-4 weeks (Fig. S1H). BSA supplementation allowed PDAC cell adaptation to glutamine limitation, as previously reported[14] (Fig.S1I). However, Glu-limitation adapted cells (in the presence of 5% BSA) proliferate slower than naïve control (Fig. S1J). Although MiaPaCa-2 cells were able to proliferation under Trp limitation conditions for up to 4 weeks, those cells stop proliferating after 4 weeks (Fig. S1J). Therefore, our data suggested that PDAC CLSA induced a unique adaptation mechanism to promote PDAC cell proliferation and tumor growth.

**CLSA cells downregulate iron sulfur cluster synthesis to promote glycolysis.**

A major function of Cys is to be used for GSH synthesis, which is required for antioxidant response and ferroptosis resistance. Acute $Cys_2$ limitation (25 μM) markedly reduced GSH levels by fifty to ninety percent in PDAC cells (Fig. S2A), which is consistent with the induction of ferroptosis by acute CLS. However, in CLSA-25 PDAC cells GSH levels were comparable to that of naïve control cells (Fig. S2A), despite little to no recovery in intracellular Cys. To understand the effects of CLSA on Cys metabolism, we used $^{15}N_2$, $^{13}C_6$-cystine to label Cys metabolites in MiaPaCa-2 cells. Control or CLSA-25 cells were incubated with 200 μM (for control) or 25 μM (for CLSA-25) $^{15}N_2$, $^{13}C_6$- $Cys_2$ for 0, 2 or 4 hours. The fractional labeling of M+4 Cys reached 68% at 2 hours and plateau after that in the control group (Fig. 2A). The M+4 Cys fractions in CLSA-25 group were 54% and 38% at 2 and 4 hours, respectively. Despite lower fractional labeling of M+4 Cys in CLSA-25 cells, the fractional labeling of GSH and GSSG levels in the two

group were similar (Fig. S2B), which suggested faster turnover of GSH/GSSG in CLSA-25 cells. Interestingly, the steady-state labeling of Cys, GSH, GSSG and CoA all decreased in CLSA-25 cells after 24 hours incubation with $^{15}N_2$, $^{13}C_6$- $Cys_2$ (Fig. S2C), which suggested that CLSA-25 cells might increase its Cys uptake from alternative sources, such as macropinocytosis and the transsulfuration pathway[14,32].

We noted that the labeling of M+4 Alanine was dramatically reduced in CLSA-25 cells (Fig. 2B). Alanine is a by-product of Cys desulfurase NFS1, which uses Cys as substrate for the synthesis of Fe-S[33]. Fe-S is a critical co-factor for oxidoreductases such as aconitase (ACO) and mitochondrial respiratory complexes I, II and III[33]. We confirmed that the activities of ACO1 and ACO2 were markedly reduced in CLSA-25 PDAC cells (Fig. 2C). The protein levels of NDUFS1, a Fe-S binding subunit in complex I, was downregulated in all the CLSA-25 PDAC cells. The down regulation of Fe-S proteins in complex II (SDHB) and complex III (RISKE) was also observed in some CLSA cells (Fig. 2D). These observations are consistent with the notion that loss of Fe-S destabilized these proteins. Mitochondria stress test showed that CLSA cells markedly downregulates mitochondrial oxygen consumption rates (OCR) while upregulating extracellular acidification rate (ECAR) (Fig. 2E-2F). Glucose uptake was also dramatically upregulated in CLSA cells (Fig. 2G). Our data suggest that by downregulating Fe-S synthesis, CLSA cells promote a switch from mitochondrial oxidative phosphorylation to glycolytic metabolism.

**Metabolic reprogramming in CLSA cells activates PPP metabolism and nucleotide synthesis.**

To gain comprehensive understanding of the CLSA-induced metabolic reprograming, we performed metabolomics screening using control and CLSA-25 PDAC cells (MiaPaCa2 and PANC1). As shown in Fig. 3A, metabolic set enrichment analysis (MSEA) showed that Warburg effects, Glycolysis, Pentose phosphate pathway (PPP) and nucleotide metabolisms (both Purine and Pyrimidine) were among the most overrepresented metabolic pathways in CLSA-25 MiaPaCa-2 and/or PANC-1 cells.

Nucleotides are critical building blocks required for the synthesis of rRNA, mRNA and DNA in proliferating cells[15]. PPP is a glycolysis shunt pathway that provides R5P and PRPP (Phosphoribosyl pyrophosphate), which are essential precursors for the synthesis of both purine and pyrimidine nucleotides[15,34]. CLSA-25 cells have increased levels of multiple ribonucleotides and deoxyribonucleotides (Fig. 3B and Fig. S3A-S3B). To determine whether CLSA activates PPP and *de novo* nucleotide synthesis, we used [U-$^{13}$C]-glucose and LC-MS/MS to analyze the effects of CLSA on the glucose entry into glycolysis and PPP metabolism (Fig. 3C-3E). As shown in Fig. 3D and 3E, CLSA increases glucose flux into glycolytic metabolites (Fig. 3E), PPP metabolites (R5P, PRPP) and nucleotides (IMP, UMP) (Fig. 3E). Our data suggest that CLSA-mediated metabolic reprograming promotes glycolysis, PPP and *de no* nucleotide synthesis to support cancer cell proliferation and tumor growth.

**OxPPP is translationally upregulated in CLSA PDAC cells to promote nucleotides and NADPH synthesis**

G6PD and TKT (transketolase) are the first and rate limiting enzymes for the oxidative and reductive PPP, respectively. Given the importance of *de novo* nucleotides synthesis in cell proliferation, we evaluated the effects of a G6PD inhibitor (G6PDi1) and a TKT inhibitor (Oxythiamine) on proliferation of CLSA25 and naïve PDAC cells. As shown in Fig. S4A-S4B, G6PDi1 abrogated CLSA-mediated cell proliferation in MiaPaCa-2 and PANC1 cells, while Oxythamine had no effect. CLSA PDAC cells were also more sensitive to G6PDi1-induced cell

death (Fig.S4C). To determine whether OxPPP might be upregulated by CLSA, we evaluated the protein expression levels of G6PD, PGLS and PGD in CLSA-25 PDAC cells and CLSA-I PDOs. As shown in Fig. 4A, G6PD protein levels were increased in all the CLSA-25 cells and CLSA-I PDOs when compared to their naïve controls. The expression of PGLS and PGD were upregulated in PDAC cells and PDOs except for MiaPaCa2 (for PGLS) and Capan-2 (for PGD) (Fig. 4A). Intriguingly, the CLSA cells retained elevated G6PD/PGD expression, cell proliferation and ferroptosis resistance even after being cultured in $Cys_2$-replete (200 uM) medium for a month (Fig. S4D-S4F), which suggested that the CLSA-mediated PPP upregulation, once established, no longer depends on external CLS.

To determine whether CLS in the PDAC patient tumor microenvironment might also lead to PPP upregulation, we stained G6PD and PGD in PDAC tissues and paired para-tumor normal tissue from 18 patients. As shown in Fig. 4C-4D, the expression levels of G6PD and PGD were robustly upregulated in PDAC tissues when compared to paired para-tumor pancreatic tissues. To investigate whether OxPPP upregulation might contribute to PDAC progression, we further determined the expression levels of G6PD in PDAC tissues from a cohort of 100 patients. As shown in Table S1, G6PD high patients had larger tumor size, more advanced TNM stages and higher incidence of lymph node metastasis (Table S1). G6PD high patients also had lower overall survival and relapse free survival (Fig.S4G), which indicates a critical role for OxPPP in PDAC tumor growth and progression.

Next, we investigated the mechanism underlying CLSA-mediated OxPPP upregulation in PDAC. We found no significant changes in the mRNA transcript levels of the three genes in this pathway (G6PD, PGLS and PGD) in CLSA-25 cells (Fig.S4H). G6PD is a very stable proteins, with no detectable degradation even after 24 hours cycloheximide (CHX) treatment (Fig.S4I). Therefore, we hypothesized that OxPPP enzymes might be translationally regulated in CLSA PDAC cells. We used L-Azidohomoalanine (AHA) to label newly translated proteins in CLSA-25 and naïve MiaPaCa2 and PANC-1 cells[35]. The labeled peptides were tagged using a biotin-alkyne click-chemistry probe. After pull-down with streptavidin, the abundance of AHA-labeled G6PD, PGLS and PGD was determined by Western blotting. The levels of newly translated G6PD and PGD were 2- to 5-fold higher in CLSA MiaPaCa-2 and PANC1 cells when compared to control (Fig. 4E). AHA-tagged PGLS only increased in CLSA-25 PANC-1 cells, but not in MiaPaCa-2 cells (Fig. 4E), which is consistent with the PGLS expression pattern in these cells.

To further investigate the translational regulation of PPP enzymes, a sucrose gradient polysome profiling experiment was carried out (Fig. 4F and 4G). Polysome profiles showed an overall shift of mRNA into heavier polysomes in CLSA25 MiaPaCa-2 cells (Fig. 4F), which indicated upregulation of translational initiation. The mRNA peak of G6PD and PGD shifted from fraction 3 in control cells to fraction 6 and 4, respectively, in CLSA25 cells showing that the number of ribosomes associated with those mRNAs is higher in CLSA25 compared with control cells. In contrast, the peak of PGLS and GAPDH shifted toward lighter fractions, which is consistent with AHA labeling results in MiaPaCa-2. The shift toward heavier polysomes for the mRNAs of G6PD and PGD suggests that OxPPP is translationally upregulated in CLSA cells.

To investigate the role of OxPPP in CLSA-mediated phenotypes, we used siRNA to knockdown G6PD in PDAC cells. Both nucleotide levels (Fig. 4H-4I) and NADPH/NADP+ ratios (Fig. 4J) were increased in CLSA25 PDAC cells, which was suppressed by siRNA depletion of G6PD (Fig.4H-4J and Fig. S4J-S4K). G6PD siRNA also inhibited the CLSA-mediated increase in ferroptosis resistance and cell proliferation (Fig. S4L-S4M). To determine whether activation of OxPPP is sufficient to mediate CLSA phenotypes, we overexpressed G6PD in naïve PDAC cells

(Fig. S4N). G6PD overexpression increased ferroptosis resistance in PDAC cells, while cell proliferation was not affected by ectopic G6PD (Fig. S4O). Taken together, our data suggested that activation of OxPPP is at least partially responsible for CLSA-mediated nucleotide synthesis, cell proliferation and ferroptosis resistance.

**CLSA promotes lipogenesis and lipid droplet formation in PDAC.**

OxPPP has been implicated in promoting lipogenesis in adipocytes and cancer cells[17,36]. NADPH, along with malonyl-CoA, is required for *de novo* fatty acid synthesis by fatty acid synthase and suppression of OxPPP inhibits lipogenesis in cancer cells[17,18]. To determine the effects of CLSA on PDAC lipid metabolism, we performed untargeted lipidomic screening using naïve and CLSA-25 MiaPaCa2 cells (Fig. 5A-5B). Triacylglycerides (TG) and ceramides (Cer) were the most upregulated and most downregulated lipid species, respectively, in CLSA-25 cells (Fig. 5A-5B). TG are the main component of LD that serve as energy and lipid storage in the cell. We confirmed through thin layer chromatography (TLC) that TG was upregulated in CLSA-25 PANC-1 and MiaPaCa2 cells (Fig.5C-5D). Confocal microscopy and flow cytometry quantitation indicated that CLSA promotes LD formation (Fig. 5E-5G). G6PD overexpression (OE) in naïve MiaPaCa-2 and PANC-1 cells was sufficient to increase TG and LD levels (Fig. S5A-S5D). Conversely, G6PD knockdown in CLSA PDAC cells significantly decreased TG levels (Fig. 5H-5I). These data suggested that CLSA promotes lipogenesis and LD formation through activation of the OxPPP.

To determine whether LD formation is upregulated in PDAC, we perform LD staining in PDAC tissue cryosections from 30 patients. LD staining in PDAC patient tissues and paired para-tumor normal tissues revealed dramatic increase in LD formation in tumor tissues (Fig. 5L-5M). In PDAC tissues LD almost exclusively colocalize with CK19 positive PDAC cells, but not with α-SMA positive cancer-associated fibroblast cells (Fig. S5E). Taken together, our data indicate that OxPPP upregulation in CLSA PDAC promotes lipogenesis and LD formation.

## Discussion

Cys and $Cys_2$ are among the most depleted amino acids in the PDAC tissues and there is intense interest in developing $Cys_2$ deprivation agents as potential anti-cancer therapies. However, the effects of chronic CLS adaptation on cancer cells and the underlying mechanisms are poorly understood. Our data provide important insights into the CLSA in PDAC. CLSA PDAC cells can maintain GSH synthesis despite severe reduction in intracellular Cys. This is remarkable since GSH levels in the PDAC cell are 20-300 fold higher than Cys. Among the major Cys metabolites Fe-S was the most severely downregulated in CLSA cells, which resulted in the downregulation of mitochondrial OXPHOS and upregulation of glycolytic metabolism.

All the CLSA PDAC cells and PDOs proliferated faster in the culture and grew into larger xenograft tumors when implanted orthotopically. Consistent with the elevated cell proliferation, CLSA PDAC cells increase *de novo* nucleotide synthesis and lipogenesis. This is at least in part due to the translational upregulation of the OxPPP pathway, which supplies R5P and NADPH for nucleotide and lipid anabolism, respectively. While genetic or pharmacological inhibition of G6PD abrogated the CLSA-mediated phenotypes, ectopic expression of G6PD could only partially recapitulate some of the CLSA phenotypes (e.g. ferroptosis resistance, lipogenesis), but not others (e.g. cell proliferation). These findings implicated the involvement of other metabolic pathways in

addition to OxPPP during CLSA. It was recently reported that PDAC cells that adapted to glucose and glutamine limitation also exhibited enhanced cell proliferation[37]. However, we found very few surviving PDAC cells under glutamine limitation conditions in the absence BSA supplementation, which is consistent with earlier reports[14]. Tryptophan and arginine are two other amino acids severely depleted in the PDAC miroenvironment[13]. We found that although PDAC cells were able to adapt to tryptophan limited cell culture medium over a period of 2-4 weeks, adapted cells proliferated slower in their respective nutrient limited media and eventually stop growing beyond 4 weeks. These findings indicate that CLS might induced unique adaptation mechanisms not shared by the deprivation of other amino acids.

It is interesting to note that CLSA induced responses, including promotion of glycolysis, nucleotide synthesis, lipogenesis, tumor growth and metastasis, are phenotypically similar to tumor response to hypoxia. Our data suggested that much like hypoxia response, nutrient limitation stress in the tumor microenvironment could also play an important role in promoting tumor growth and progression.

## Materials and Methods

### Antibodies, key reagents and inhibitors

Information for antibodies, key reagents and inhibitors are included in Table S2 and S3.

### Cell culture

The PDAC cell lines (MiaPaCa-2, PANC-1, SW-1990, Capan-2) were obtained from the ATCC. KPC cells were derived from *Kras*$^{lsl\text{-}Kras\ G12D/+}$; *Trp53*$^{R172H/+}$; *Pdx1-Cre* (KPC) genetically engineered mouse model. Pan02 cell was a gift from Dr. Shari Pilon-Thomass (Moffitt Cancer Center). All ATCC cell lines were characterized or authenticated by the ATCC using short tandem repeat profiling and passaged in our laboratory for fewer than 6 months before use. All cell lines used were free of microbial (including mycoplasma) contamination. We routinely perform test for mycoplasma contamination in the lab at least montly. All pancreatic cells were cultured in DMEM medium supplemented with 10% fetal bovine serum and 1% Penicillin-Streptomycin and maintained at 37 °C in a humidified 5% $CO_2$ incubator.

### Induction of CLSA

CLSA-25 and CLSA-50 cell culture media were prepared by supplementing pyruvate, glutamine, methionine and cystine-free DMEM media (Gibco, 21013-024) with 1 mM Sodium Pyruvate, 4 mM glutamine, 200 uM L-Methionine and 25 uM L-cystine (for CLSA25) or with 50 uM L-cystine (for CLSA50). To induce CLSA, PDAC cells were cultured in indicated L-cystine limited media supplemented with 10% FBS and 1% Penicillin-Streptomycin for 4 weeks. The media were changed every other day during this period. After 4 weeks adaptation, cells were frozen and stored in liquid nitrogen. After recovery from liquid nitrogen cells were cultured in their respective induction media and used for experiments within 6 passages.

### Patient derived organoid (PDOs) culture

PDO were derived and cultured following a previosly described protocol [30]. To induce CLSA-I PDO, two PDOs were cultured in medium containing 0.5 uM IKE (Imidazole ketone erastin) for 4 weeks. For PDO xenografts, CLSA-I or control PDOs were digested into single cells using TrypLE Express and then neutralized with Human Complete Feeding Medium (hCPLT) contained Human Wash Medium with BSA (Advanced DMEM/F-12, 10mM HEPES, 1 × GlutaMAX

Supplement, 100μg/ml Primocin and 0.1% BSA). $1\times10^5$ of PDO cells were resuspected into Matrigel and injected orthotopically into pacreas. The growth of tumors were monored through MRI scan using 9.4 T MR scanner (Bruker BioSpec 94/30 USR) at Multimodality Preclinical Molecular Imaging Center in Tianjin Medical University General Hospital. The tumor volume was calculated with the formula: volume = length × width × width/2.

**Treatment of PDAC cells and PDOs with modified FOLFIRINOX (mFOLFIRINOX)**

mFOLFIRINOX Treatment of PDAC cells and PDO cultures were carried out as previously described. The mFOLFIRINOX cocktail consisted of 5-FU, SN-38 (metabolic product of Irenocan responsible for its inhibitory activity toward DNA topoisomerase I) and oxaliplatin at a 2:1:2 ratios. The indicated mFOLFIRINOX concentrations were the concentrations of 5-FU and oxaliplatin.

**Cell proliferation assay**

$1x10^5$ Cells per well were seeded onto a 12-well plate in triplicate. The media were changed every two days. At indicate time points, the cells were fixed with 10% formalin for 15 min and stained with 0.5 mL 10% crystal violet solution for 20 min with shaking. After staining, the cell were washed with water for five times and dried overnight. The crystal violet staining was solubilized with 1 ml 10% acetic acid absorbance at OD 590 nm was determined with a plate reader.

**Cell viability assay**

$1\ x10^4$ cells per well were seeded onto 96-well plates (Corning, 3610) and treated with different drugs at indicated concentrations for two to three days. Cell viability were tested using CellTiter-Glo Cell Viability Assay (Promega, G7572) and recorded as relative luminescence units (RLU) using FlexStation 3 (Molecular Devices).

**2-NBDG Glucose uptake assay**

PDAC cells were seeded at $2 \times 10^5$ cells / well in a12 well plate. The cells were incubated with 500 μL of culture medium containing 50 μM 2-NBDG and incubated at 37 °C for 2 h. The reaction was terminated by washing the cells twice with ice cold PBS. The cell was re-suspended through trypsinization and analyzed through flow cytometry using the excitation/emission at 467/542 nm.

**Mitochondria stress test and glycolysis stress test.**

Oxygen consumption rate (OCR) and extracellular acidification rate (ECAR) were determined using Seahorse XFe24 Extracellular Flux Analyzer (Agilent Seahorse Bioscience) following protocols recommended by the manufacturer. Cells were seeded on XF24 cell culture microplates (2.5*10^5 cells/well). Cells were maintained in a XF DMEM assay medium (Agilent, 103575-100) in a non-$CO_2$ incubator for 30 min before the assay. The XF Cell Mito Stress Test Kit (Agilent, 103015-100), was used for the OCR assay. XF Glycolysis Stress Test Kit was used for the ECAR assay (Agilent, 103020-100). For mitochondria stress test, the baseline recording was followed by sequential injection the following reagent to the final concentration: 1.5 uM oligomycin, 1 uM FCCP, and 0.5 uM rotenone/antimycin A. For glycolysis stress test, the baseline recording was followed by sequential injection the following reagents: 10 mM D-glucose, 1 uM oligomycin, and 50 mM 2-DG.

**RNA interference and other constructs**

The knockdowns of G6PD, DGAT1 and DGAT2 was achieved using the 27mer duplexes DsiRNA system from IDT. The targeting sequences are listed in Table S4. pLX304-G6PD was constructed by subcloning the human G6PD cDNA into pLX304 vector through Gateway subcloning. The lentiviral particles were packaged in HEK293 cells using the PEI transfection method, and concentrated as previously described [38]. After selection with blasticidine, the surviving cells were pooled together and used for assays.

**Western blotting**

Cells were lysed in SDS-NP40 buffer (50 mM Tris, pH 8.0, 150 mM NaCl, 1% NP40, 1% SDS, 1mM protease inhibitors cocktail) on ice for 1 min. Cells were scraped from the plate and sonicated briefly for three times. Then lysates were centrifuged at 20,000 ×g, 4 °C for 10 min. 20-40 µg proteins were separated by SDS-PAGE and transferred onto PVDF membrane. The membranes were incubated in blocking buffer (5% (w/v) nonfat dry milk in Tris-buffered saline, 0.05% Tween 20 (TBS-T)) for 30 min at RT., and incubated with primary antibodies for 20 h at 4 °C, followed by incubation with secondary antibodies for 60 min at RT. Antibody information are listed in Supplementary Table S4.

**Reverse transcription-polymerase chain reaction**

$1\times10^6$ cells were washed with ice-cold PBS and total RNA was extracted using RNeasy kit (Qiagen, Cat#74106). 1 µg RNA was used for the reverse transcription using High-Capacity cDNA Reverse Transcription Kit (Thermo Fisher Scientific, 4368814). cDNA was diluted 1:10 then used for qPCR with ABI qPCR master mix (Thermo, Cat#4367659). Each RT-PCR experiment was performed independently at least three times. The PCR primers used are listed in Supplementary Table S5.

**L-Azidohomoalanine (AHA) labeling of OxPPP enzymes.**

$7x10^6$ cells on a 10 cm dish were rinsed twice with 5 ml 1xPBS and incubated with L-Met free DMEM medium for 1 hour in 37°C, 5% $CO_2$ incubator. After 1 hour, L-AHA were added to the final concentration of 1 mM. After 1 hour labeling with AHA, cells were lysed. To label newly-synthesized proteins, lysate was mixed with 2x click-chemistry reaction buffer (2 mM Copper Sulfate, 20 uM Biotin-Alkyne, 2 mM TCEP in 1xPBS) and incubated for 60 minutes at room temperature with shaking. The reaction was terminated by adding TCA to the final concentration of 10% and incubated on ice for 30 minutes. After 10,000 g centrifugation at 4°C 10 minutes, the precipitate was washed with 1ml ice-cold acetone for 3 times, and air-dried at room temperature for 30 minutes. The pellet was re-dissolved in 500 ul RIPA buffer with proteinase inhibitor cocktail and sonicated for 10 seconds on ice 3 times. The biotin-labeled proteins were precipitated with 40 ul NeutrAvidin resin and affinity-purified OxPPP enzymes were detected with Western blotting using antibodies for G6PD, PGD, PGLS and with GAPDH as control.

**Polysome profiling**

$1x10^7$ cells were treated with cycloheximide (100 ug/ml) in the cell culture media for 2 minutes and the cells were placed on ice. After removal of media, the cells were washed twice with ice-cold 1xPBS/cycloheximide (100 ug/ml). Cells were scraped in 600 ul Polysome Buffer (50 mM HEPES, pH 7.4, 250 mM KCl, 5 mM $MgCl_2$, 250 mM sucrose) containing 1% Triton x-100, 1.3% NaDOC, 100 ug/ml cycloheximide, 0.1 U/ul SUPERase. In RNAase inhibitor (AM2694, Invitrogen). After 10 minutes lysis at 4°C with rocking, the lysates were centrifuged at 3,000 g for 15 minutes at 4°C. 600 ul supernatant was loaded to a sucrose gradient (20%-47%, w/w) and

centrifuged in a Beckman SW41Ti rotor at 34,000rpm for 160 minutes at 4°C. After centrifugration, 8 fractions were collected from each. The RNA from each fraction was extracted using TRlzol (15596018, Invitroen) and used for qPCR analysis.

**LC-MS/MS analysis of NEM-cysteine, GSH, dNTP and NADP+/NADPH**

*NEM-cysteine*: The measurement of NEM-derivatized cysteine in pancreatic cancer cells was carried out following our previously reported protocol [30]. For preparation of human and mouse tissue samples, 10 mg PDAC or para-tumor normal tissues were immersed in 10 ul NEM Tissue Buffer (25 mM N-Ethylmaleimide, 10 mM Ammonium Formate, pH7.0) spiked with 10 uM NEM-$^{15}N$,$^{13}C_3$-Cysteine as interior control) and homogenized with a glass Dounce tissue homogenizer on ice. The homogenate was centrifuged at 20,000 rpm, 4°C for 5 minutes and 5 ul supernatant were diluted in 45 ul NEM Tissue Buffer and used for LC-MS/MS analysis.

*GSH*: $2x10^5$ cells in 12 well plate (70% confluency) were washed with ice cold 1xPBS three times and the residual PBS was thoroughly removed. 225 ul ice-cold 0.1% formic acid and 25 ul [$^{13}C_2$,$^{15}N$] GSH (1ug/ml in 0.1% formic acid) was added to the well. The cells were scrapped in to a 1.5 ml Eppendorf tube. Cells were vortexed for 15 seconds, snap-frozen in liquid nitrogen for 1 minute and thawed in a room temperature water bath. After three freeze-thaw cycle, cells were centrifuged at 13,000 g for 3 minutes and the supernatant were collected for LC-MS/MS analysis.

dNTP: $1x10^6$ cells (in 6-well plate) were washed with ice-cold PBS and residual PBS was removed. 490 ul ice-cold 80% MeOH spiked with 10 ul 100nM [$^{13}C_{10}$,$^{15}N_5$]-dATP (646237, Sigma) internal standard were added and cells were scrapped into a 1.5 mL tube. After vortex, the lysates were centrifuged at 21,130 g, 4°C for 10 min. The supernatant was transferred to a new tube and mixed with 1 ml 50 mM $NH_4Ac$, pH 4.5 and used for subsequent SPE. Oasis WAX 1 cc, 30 mg, 30 um cartridge (Waters, Milford, MA, USA) was used for SPE. The cartridge was activated with 1 ml methanol, and equilibrated with 1 ml $dH_2O$ prior to sample loading. After the samples loading by gravity, the cartridge was washed by 1 mL 50 mM $NH_4Ac$, pH 4.5, and 1 mL 0.5 % (25 % $NH_4OH$) in methanol. The analytes were finally eluted with 1 ml buffer containing 80 % methanol, 15 % water and 5 % (25% $NH_4OH$). The eluent was dried by Speed-vac and reconstituted with 50 ul reconstitution solution for LC-MS/MS analysis.

*NADP+/NADPH:* $1x10^6$ cells in 6-well plate were washed with ice-cold PBS and extracted with 0.4 ml 80% MeOH pre-chilled to -20°C. The plates are transferred to -80°C for 15 minutes and cells were scrapped into a 1.5 ml tube. After centrifugation at 15,000 g for 10 minutes at 4°C, the supernatant was used directly of LC-MS/MS analysis.

*LC-MS/MS:* All LC-MS/MS analysis were carried out using Sciex QTRAP 6500+ mass spectrometry coupled with a Sciex EXion HPLC separation system. The multiple reaction monitoring mode (MRM) was used to analyze and quantify metabolites. All peaks were integrated and quantified by Sciex OS 3.0 software.

**Patients tissue specimens**

Tumor samples and para-tumor normal tissues were obtained from 100 patients with PDAC treated at the Tianjin Cancer Hospital from 2014 and 2018. All ?? patients underwent radical pancreaticoduodenectomy with R0 margins confirmed by two pathologists. None of the patients had received chemotherapy or radiotherapy at the time of sample collection. All patients were treated with systemic gemcitabine-based chemotherapy after operation for six cycles after surgery. No radiotherapy was given before or after surgery. Postoperative follow-up of patients were

conducted every 3 months initially. Overall survival (OS) was defined as the time interval from the date of surgery to that of death due to any cause or that of the last follow-up. Relapse-free survival (RFS) was calculated from the date of surgery to that of local recurrence or metastasis. Local recurrence or metastasis was diagnosed by radiological examination (contrast-enhanced CT or MRI scanning). All patients provided written informed consent. The study protocols were approved by the Ethics Committee of the Tianjin Cancer Institute and Hospital.

**Orthotopic xenograft and bioluminescence imaging (BLI)**

The orthotopic PDAC xenograft and BLI imaging were carried out following previously reported procedures[30,39,40] according to IACUC protocols approved by the IACUC committee at the Penn State College of Medicine or Tianjin Cancer Hospital. Briefly, Luciferase labeled PDAC cells ($1x10^5$ for KPC and Pan02 cells, $1x10^6$ for MiaPaCa-2 cells) were resuspended in 20 ul Matrigel (diluted in DMEM media) and orthotopically injected into carefully exposed pancrease of 6-7 weeks old female mice (C57BL/6J for KPC and Pan02 cells, BALB/c Nude mice for MiaPaCa-2 cells). The wound was closed with suture and wound clip. Non-invasive BLI imaging was carried out using Xenogen IVIS 200 1 week after the surgery to monitored the orthotopic tumor growth. At the end of the experiment, liver were inspected for visible metastatic lessions and ex vivo BLI imaging was carried out to monitor liver metastasis.

**IHC analysis**

Sections of formalin-fixed, paraffin-embedded tumors were subjected to IHC analysis for G6PD and PGD as using a DAB (3,3'-diaminobenzidine) substrate kit (Maixin) according to the manufacturer's instructions. Sections were incubated with anti-G6PD (sc-373886, Santa Cruz Biotechnology, at 1:200 dilution) or anti-PGD (sc-398977, Santa Cruz Biotechnology, at 1:200 dilution) antibodies overnight at 4°C. After wash, the sections were stained with a secondary antibody for 30 minutes at room temperature. PBS was substituted for each primary antibody as a negative control. Five random fields were examined under a light microscope. Immunoreactivity was semiquantitatively scored according to the estimated percentage of positive tumor cells as described previously. IHCstaining results were blindly and independently performed by two pathologists who were blinded to the clinical data. Staining intensity was scored 0 (negative), 1 (low), 2 (medium), and 3 (high). Staining extent was scored 0 (0% stained), 1 (1%–25% stained), 2 (26%–50% stained), and 3 (51%–100% stained). The final score was determined by multiplying the intensity scores with staining extent and ranged from 0 to 9. Final scores (intensity score x percentage score) less than or equal 4 were considered as low staining, more than 4 were high staining. Antibodies used in IHC staining can be found in Supplementary Table S5.

**Lipid droplets staining**

For the staining of lipid droplets in tissues, we subjected fresh cancer/cancer-adjacent tissues from patients or mouse tumor fragments to rapid freezing, followed by embedding in OCT compound and sectioning. The sections were stored at -20°C. Prior to staining, the sections were gradually thawed at 4°C for 20 minutes, then permeabilized with ice-cold acetone for 20 minutes. Afterward, sections were blocked with 3% BSA for 30 minutes. Subsequently, BODIPY™ 493/503 NHS ester (succinimidyl ester) dye was added at a final concentration of 5 μM for the staining of adiposomes. The sections were incubated at room temperature for 60 minutes, washed three times with PBS, and counterstained with DAPI. For quantitation, The average LD numbers per cell from 5 random fields (20x objective) were counted.

For lipid droplet staining in cells, $3x10^5$ cells were seeded onto a 3.5 cm glass bottom cell culture dish (50% confluency). The glass bottom was coated with 0.2% gelatin as previously described [41].

Cells were stained with 1.5 ul LipidSpot™-488 dye diluted in 1 ml cell culture medium in a 37°C $CO_2$ incubator for 30 minutes. After staining, the cells were washed with 1xPBS and fixed with 4% paraformaldehyde for 10 minutes, washed with 1xPBS twice and counterstained with DAPI. The lipid droplets were imaged with Leica SP8 laser scanning confocal microscope equipped with an 63x oil immersion objective.

**Thin layer chromatography (TLC)**

$5x10^6$ cells in a 10 cm dish were washed with 1xPBS twice and harvested with a cell scrapper. The cell pellets were wash with 1xPBS twice and the lipids were extracted with 750 ul methanol:choloroform (4:1, v/v). After centrifugation at 13,300 rpm for 5 minutes at room temperature, the supernatant was mixed with 600 ul 0.1% aqueous acetic acid and 300 uL chloroform and vortexed for 10 seconds. The mixture was centrifuged at 13,300 rpm for 5 minutes and the lower organic phase was transferred to a glass vassel and dried under nitrogen. The dried lipids were reconsituted in choloroform and loaded onto Silica gel 60 TLC plate (1.11845.0001, Merck). The TLC plates were dervloped using hexane/diethyl ether/acetic acid 60:40:1 (v/v/v). The lipids were visualized using iodine vapor and imaged with a scanner.

**Metabolomics and lipidomics screening**

Metabolomics screening was performed through LC-MS/MS as previously described [42]. The MSEA analysis was performed using Metaboanalyst 5.0. Targeted quantitative lipidomics assay was performed with assistance from Metware Bio (Woburn, MA). $1x10^7$ cells were harvested using a cell scrapper. The cell pellets were resuspended in 100 ul $dH_2O$ containing proteinase inhibitors. 50 ul cell suspensions were used for lipid extraction while the remainding samples were used for protein assay. The data acquisition instruments consisted of Ultra Performance Liquid Chromatography (UPLC) (NexeraLC-40, Shimadzu) equipped with Thermo Accucore™C30 (2.6 μm, 2.1 mm×100 mm i.d.) column and tandem mass spectrometry (MS/MS) (Triple Quad 6500+, AB/SCIEX). Liquid phase conditions: Mobile phase: A phase was acetonitrile /water (60/40, V/V) (0.1% formic acid added, 10 mmol/Lammonium formate); B phase was acetonitrile / Isopropyl alcohol (10/90, V/V) (0.1% formic acid added, 10 mmol/L ammonium formate); Gradient program: 80:20(V/V) at 0 min, 70:30(V/V) at 2 min, 40:60(V/V) at 4 min , 15:85(V/V) at 9 min, 10:90(V/V) at 14 min, 5:95(V/V) at 15.5 min, 5:95(V/V) at 17.3 min, 80:20(V/V) at 17.5 min, 80:20(V/V) at 20 min; Flow rate: 0.35 ml/min; Column temperature: 45∘C; Injection volume: 2 μL. Mass spectrometry conditions:

LIT and triple quadrupole (QQQ) scans were acquired on a triple quadrupole-linear ion trap mass spectrometer (QTRAP), QTRAP® 6500+ LC-MS/MS System, equipped with an ESI Turbo Ion-Spray interface,operating in positive and negative ion mode and controlled by Analyst 1.6.3 software (Sciex). The ESI source operation parameters were as following: ion source, turbo spray; source temperature 500 ∘C; ion spray voltage (IS) 5500 V(Positive),-4500 V(Neagtive); Ion source gas 1 (GS1), gas 2 (GS2), curtain gas (CUR) were set at 45, 55, and 35 psi, respectively. Instrument tuning and mass calibration were performed with 10 and 100 μmol/L polypropylene glycol solutions in QQQ and LIT modes, respectively. QQQ scans were acquired as MRM experiments with collision gas (nitrogen) set to 5 psi. DP and CE for individual MRM transitions was done with further DP and CE optimization. A specific set of MRM transitions were monitored for each period according to the lipids eluted within this period.

### $^{13}C_6$, $^{15}N_2$-cystine tracing

Cystine isotopologue tracing was performed following a previously described protocol[43] with modifications. Cystine, methionine and glutamine free DMEM media (Gibco, 21013-024) were supplemented with 400 uM (for control group) or 50 uM (for CLSA-25 group) $^{13}C_3$, $^{15}N$-cysteine, 100 uM methionine, 4 mM glutamine and 10% dialyzed FBS and stored at 4°C for 48 hours for the oxidation of cysteine to cystine. $7x10^6$ control or CLSA-25 MiaPaCa-2 cells were pre-conditioned in the same medium containing $^{12}C$,$^{14}N$-cystine for 12 hours. After pre-conditioning, cells were labeled with their respective media containing isotopologue cystine for indicated time (2, 4 or 24 hours). The metabolites were extracted with 2 ml 80% MeOH. After centrifugation, the supernatant was dried under nitrogen flow and analyzed through LC-MS/MS.

### $^{13}C_6$ -glucose tracing to glycolosis and PPP/nucleotide metabolites

$^{13}C_6$ -glucose tracing was performed as we described previously with modifications [42,44]. $7x10^6$ control or CLSA-25 MiaPaCa2 cells were incubated with DMEM medium (Life technology, D98002710) containing 200 uM (for control group) or 25 uM cystine (for CLSA-25 group), 10 mM $^{13}C_6$ -glucose and 10% dialyzed FBS for indciated time (from 0-360 minutes). The supernatant was collected and dried using SpeedVac and re-dissolved in 50 µL of methanol/water (50/50) for LC-MS/MS analysis as previously described [44].

### Material availability

All unique/stable reagents generated in this study are available from the lead contact with a completed materials transfer agreement.

.

### Acknowledgement

We would like to thank the Flow Cytometry Core (RRID: SCR_021134) and Mass Spectrometry Core (RRID: SCR_017831) at Penn State College of Medicine for their technical support and Dr. Xianming Deng for critically reading the manuscript. The research in S. Yang's lab is supported by grants from the NIH (R01CA256911, R01CA233844). The research in J. Hao and X. Wang's lab is supported by grants from National Natural Science Foundation of China (grants 82430057, 82273362, 82472973).

## Figures and legends

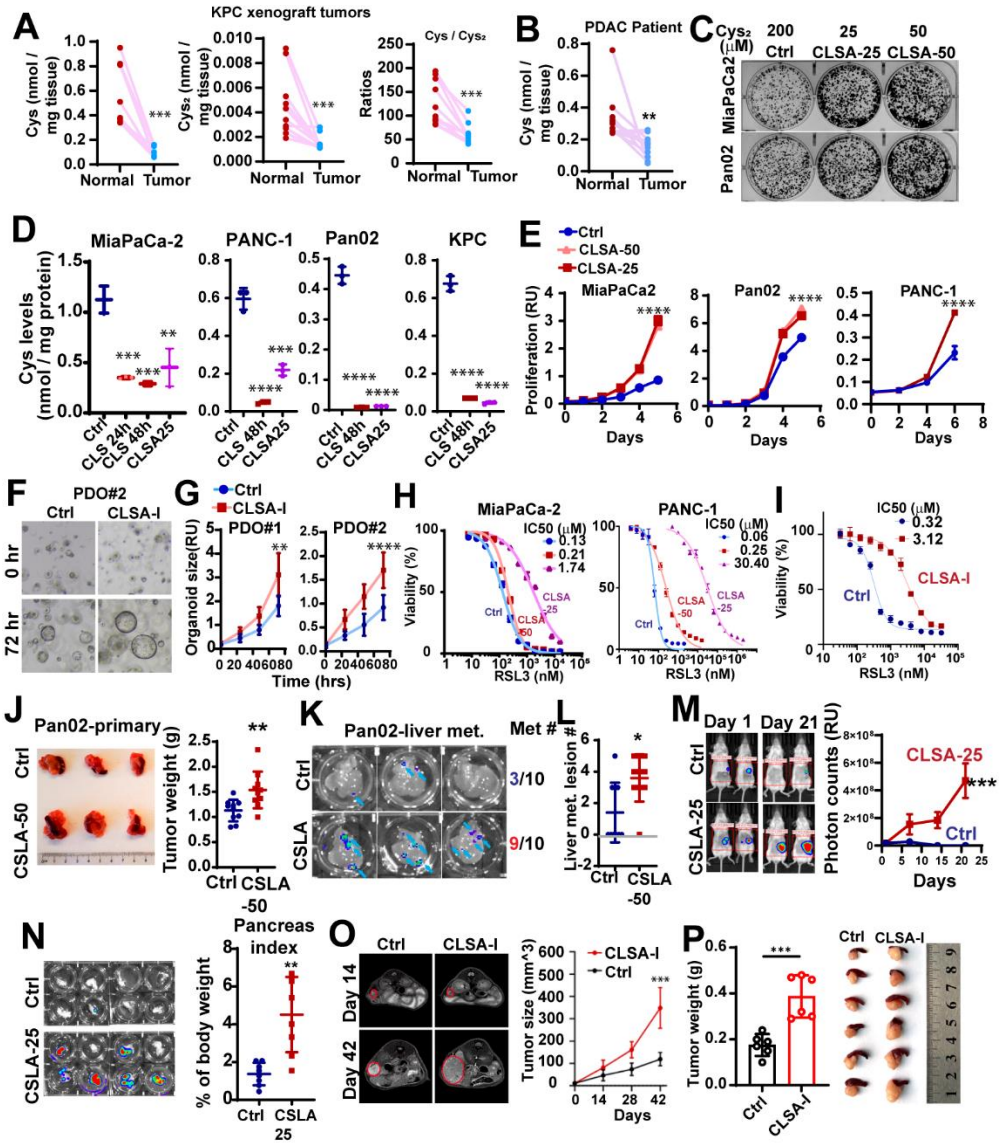


**Figure 1. Adaptation to $Cys_2$ limitation stress promotes PDAC cell proliferation and tumor growth.**

**A and B,** The levels of Cys and $Cys_2$ in PDAC tissues (tumor) and paired para-tumor normal (normal) pancreatic tissues from KPC xenograft mice (n=10) (A) and PDAC patients (n=10) (B) were determined through LC-MS/MS after NEM derivation.

**C,** The effect of CLSA on colony formation assay MiaPaCa-2 and Pan02 cells. CLSA-25 and CLSA-50 cells were cultured in $Cys_2$-limited media containing 25 uM and 50 uM $Cys_2$, respectively. Parental cells cultured in $Cys_2$ replete (200 μM) medium were used as control.

**D,** Cys levels in PDAC cells after being cultured in $Cys_2$-limited (25 uM) media for 24-48 hours, or after adaptation to 25 uM $Cys_2$-limitation for 4 weeks.

**E,** The effects of CLSA on cell proliferation in PDAC cell lines.

**F and G**, Representative bright-field microscopy (F) and quantitation (G) showing the effects of CLSA-I on tumoroid growth in two PDO models.

**H and I,** the effect of CLSA-25, CLSA-50 (H) and CLSA-I on RSL3-induced ferroptosis in PDAC cell lines (H) and PDO (I) models.

**J,** representative image (left) and quantitation of tumor weight of orthotopic xenograft tumors harvested from C57BL/6 mice implanted with control or CLSA-50 Pan02 cells (n=10)

**K,** *ex vivo* BLI imaging showing the liver metastatic lesions from mice in (J). Right, fraction of mice that developed liver metastasis in control or CLSA-50 group.

**L,** quantitation of liver metastatic lesion numbers from mice in J-K (n=10).

**M,** Representative BLI imaging from Albion BL6 mice implanted with control of CLSA-25 KPC tumor cells on day 1 and day 21. Left, quantitation of BLI imaging (phonton counts) over time. (n=10)

**N,** *ex vivo* BLI imaging (left) and the weight (right) of pancreas harvested from M (n=10).

**O,** representative MRI images (left) and quantitation of tumor volume of mice implanted with control or CLSA-I PDO1. (n=6 per group).

**P,** photos (left) and weight of pancreas (right) (n=6) harvested from mice in O.

Data in (A-B) were analyzed using two sample, two-tailed paired Stuent's t-test; data in (D)- (E) and (J)–(P) were analyzed using two-tailed, two-sample unpaired Student's t test. Data in (D)-(E) are representative results from at least three independent experiments (n = 3 biological replicates per group for each experiment). *, **, *** and **** represents $p<0.05$, 0.01, 0.001 and 0.0001, respectively.

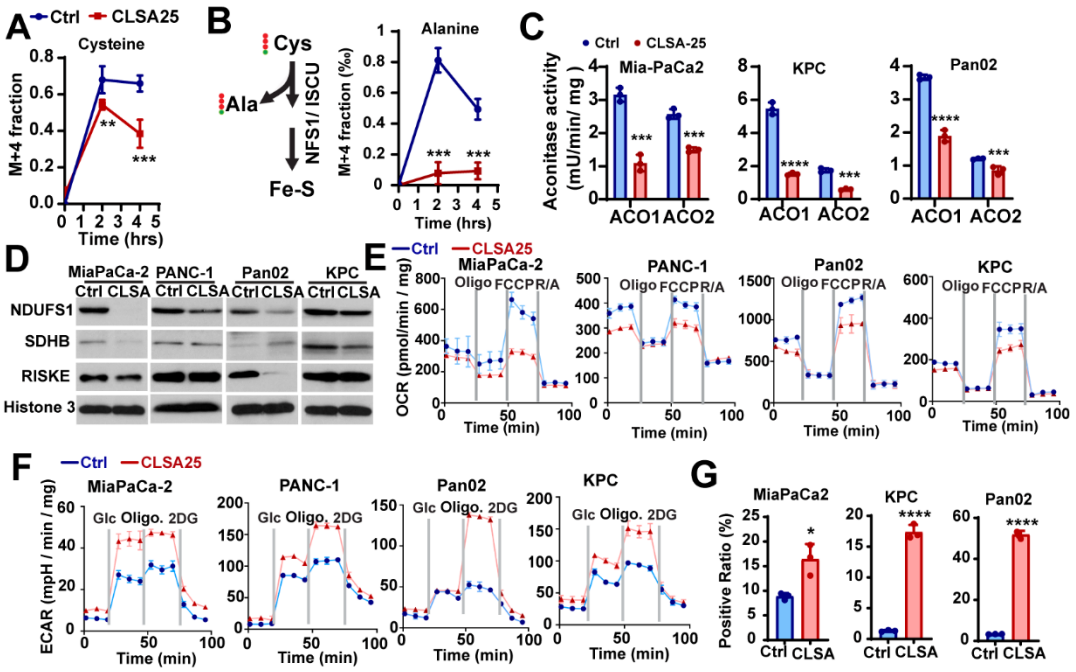


**Figure 2. CLSA cells downregulate Fe-S synthesis to promote glycolysis**

**A and B,** fractional labeling of M+4 Cys (A) and Ala (B) in control and CLSA-25 MiaPaCa-2 cells after incubation with [$^{13}C_6$, $^{15}N_2$]-$Cys_2$ for 2 or 4 hours.

**C,** the effect of CLSA-25 on aconitase 1 (ACO1) and 2 (ACO2) activities in PDAC cells.

**D,** Western blotting showing the proteins levels of Fe-S proteins in mitochondrial complex I (NDUFS1), II (SDHB) and III (RISKE) in control or CLSA-25 PDAC cells.

**E and F,** the effects of CLSA-25 on mitochondrial oxygen consumption rate (OCR) or extracellular acidification rate (ECAR) in different PDAC cell lines.

**G,** the effects of CLSA-25 on glucose uptake, as determined by 2-NBDG labeling and flow cytometry analysis, in PDAC cells.

Data in (A-C) and (G) were analyzed using two sample, two-tailed unpaired Stuent's t-test. Data in (D-F) are representative results from at least three independent experiments (n = 3 biological replicates per group for each experiment). *, **, *** and **** represents $p<0.05$, 0.01, 0.001 and 0.0001, respectively.

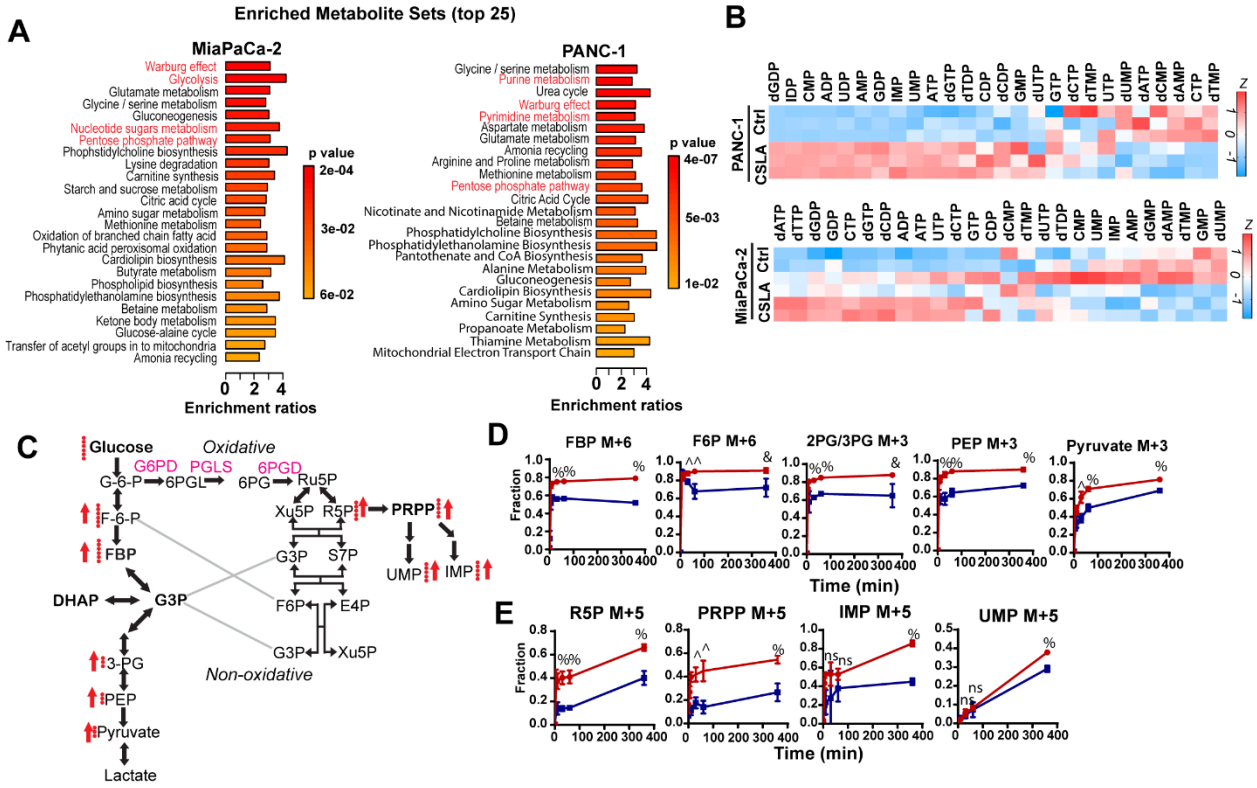


**Figure 3. Metabolic reprogramming in CLSA cells activates PPP metabolism and nucleotide synthesis.**

**A,** Metabolic Set Enrichment Analysis showing the 25 most differentially regulated metabolic pathways in CLSA-25 MiaPaCa-2 and PANC-1 cells according to targeted metabolomics screening.

**B and C,** heatmap (B) and bar graph (**C**) showing the levels of different nucleotides in CLSA-25 PANC-1 and MiaPaCa-2 cells in metabolomics screening.

**D,** Summary of $^{13}C$ incorporation into glycolysis and PPP metabolites in control and CLSA-25 MiaPaCa2 cells using [U-$^{13}C$] glucose as tracer. Red arrows indicate increases in $^{13}C$ incorporation into the indicated metabolite.

**E and F,** fractional labeling of intermediate metabolites in glycolysis (E), PPP and nucleotide synthesis pathways after tracing with [U-$^{13}C$] for indicated time.

Data in (D-E) were analyzed using two sample, two-tailed unpaired Stuent's t-test. Data are shown as mean ± SD of 5 biological repeats. *, &, ^ and % represents p<0.05, 0.01, 0.001 and 0.0001, respectively.

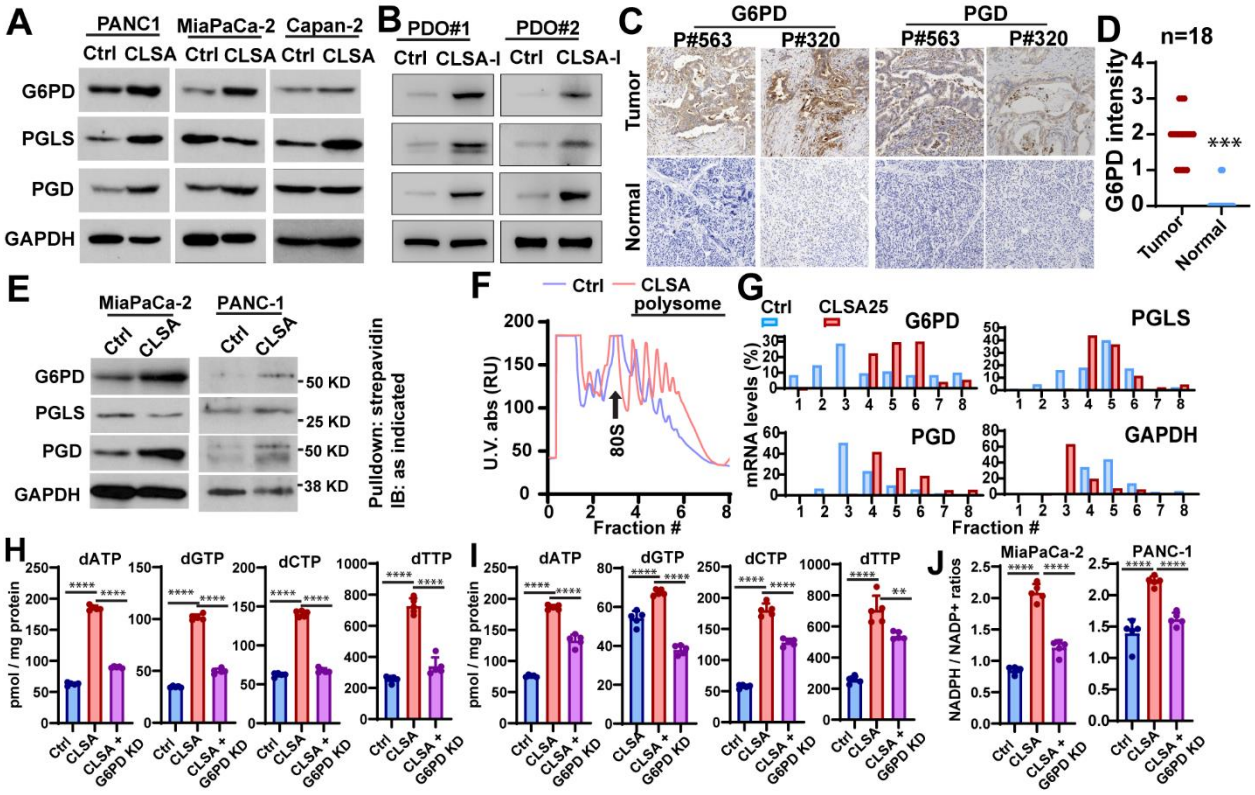


**Figure 4. Translational upregulation of OxPPP enzymes promotes nucleotide and NADPH synthesis in CLSA PDAC cells.**

**A and B,** Western blotting showing the expression of G6PD, PGLS and PGD, the three OxPPP enzymes in CLSA-25 PDAC cell lines (A) and CLSA-I PDOs (B).

**C and D,** representative IHC staining (C) and quantitation (D) showing the expression of G6PD and PGD in PDAC tumor tissues and paired para-tumor normal tissues (n=18).

**E,** AHA labeling of newly synthesized G6PD, PGD and GAPDH in Ctrl and CLSA-25 PDAC cells.

**F,** sucrose gradient polysome profiling analysis showing a shift in polysome profiles in CLSA-25 MiaPaCa2 cells (F).

**G**, qPCR analysis showing the distribution of the mRNA transcripts of G6PD, PGD, PGLS and GAPDH in CLSA-25 and control MiaPaCa2 cells.

**H and I,** LC-MS/MS quantitation of the effects of CLSA-25 and G6PD KD on dNTP levels in MiaPaCa-2 (H) and PANC-1 (I) cells.

**J,** LC-MS/MS analysis of the effects of CLSA-25 and G6PD KD on NADPH/NADP+ ratios MiaPaCa-2 and PANC-1 cells.

Data in (D) were analyzed using two sample, two-tailed Mann Whitney U-test. Data in (H-J) were analyzed using two sample, two-tailed unpaired Student's t-test. Data in (A-B) and (E-G) are representative results from at least three independent experiments. Data in (H-J) showed mean±SD of 4 biological repeats. *, **, *** and **** represents $p<0.05$, 0.01, 0.001 and 0.0001, respectively.

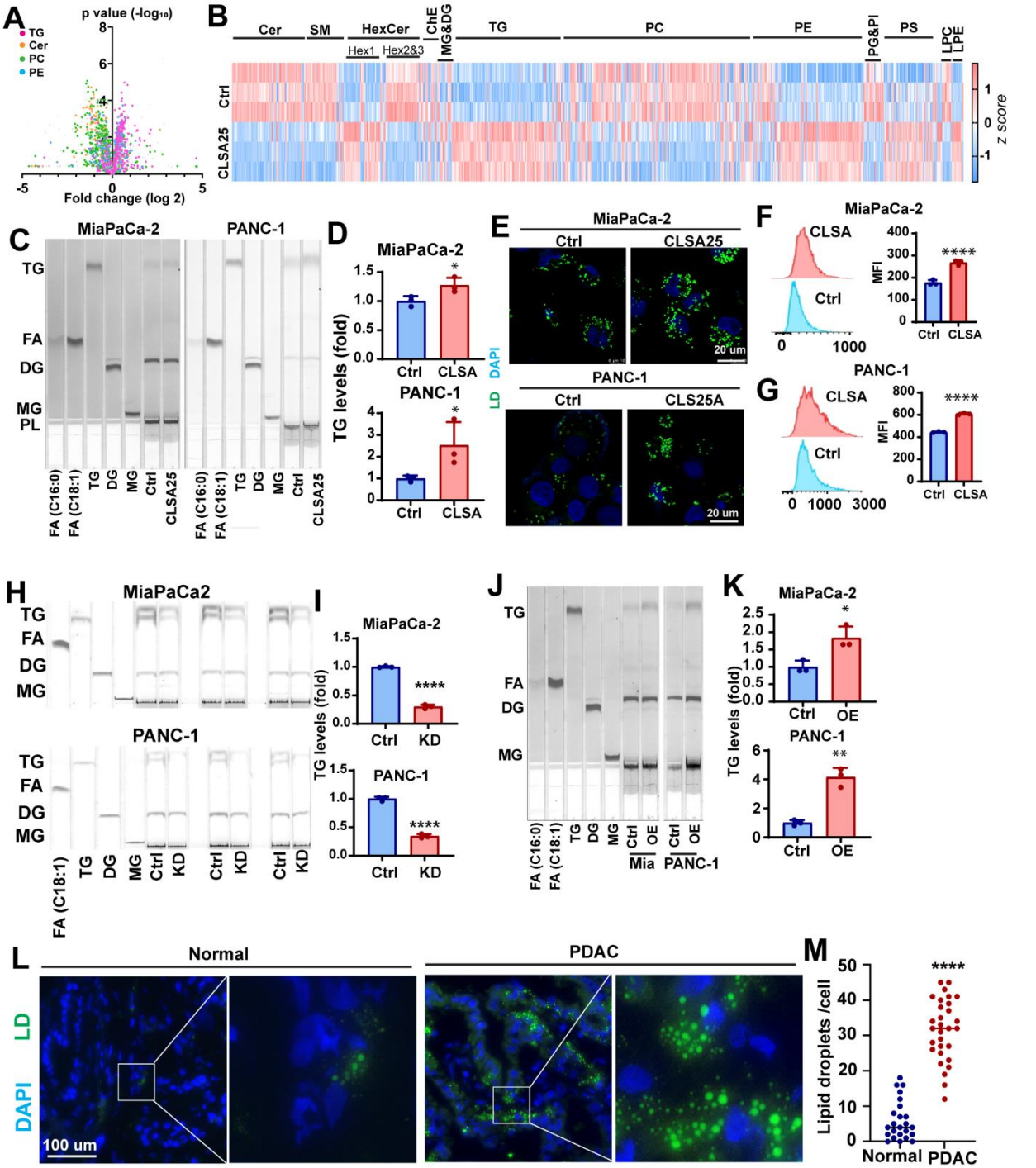


**Figure 5. CLSA-mediated lipidomics reprograming in PDAC cells promotes triacylglycerides (TG) synthesis and lipid droplet (LD) formation.**

**A and B,** volcano plot (A) and heatmap showing that CLSA-mediated lipidomics reprograming upregulates TG levels in MiaPaCa-2 cells.

**C and D,** TLC analysis (C) and densitometry quantitation (D) showing the effects of CLSA-25 on TG levels in MiaPaCa-2 and PANC-1 cells.

**E-G,** confocal microscopy imaging (E) and flow cytometry analysis (F and G)of LD staining showing upregulation of LD formation in CLSA-25 PDAC cells. Representative flow cytometry traces (left) and MFI (median fluorescence intensity) quantitation of flow cytometry data (right) are shown in F and G.

**H and I,** TLC analysis (J) and densitometry quantitation (K) showing the effects of knockdown (KD) on TG levels in CLSA-25 MiaPaCa-2 and PANC-1 cells.

**J and K** TLC analysis (J) and densitometry quantitation (K) showing the effects of G6PD ectopic expression on TG levels in naïve MiaPaCa-2 and PANC-1 cells.

**L and M,** representative confocal micrograph (L) and quantitation (M) showing LD levels in PDAC tissues and paired para-tumor normal pancreas tissues. n=30

Data in (M) were analyzed using two sample, two-tailed Mann Whitney U-test. Data in (D), (F-G), (I-K) showed mean±SD of 3 biological repeats and were analyzed using two sample, two-tailed unpaired Student's t-test. * and **** represents $p<0.05$ and 0.0001, respectively.

## Supplementary Figures and Legends

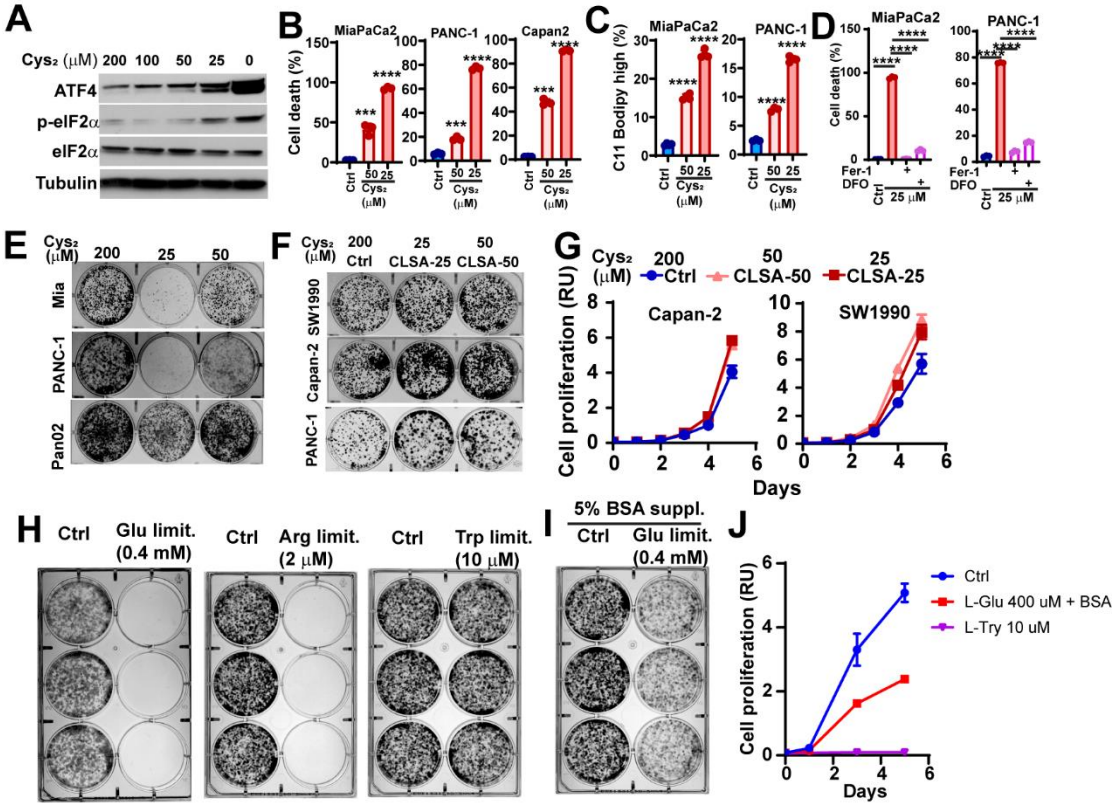


**Supplementary Figure 1. Adaptation to $Cys_2$ limitation stress promotes PDAC cell proliferation**

**A,** the effects of $Cys_2$ limitation (24 hours) on the levels of ATF4, p-eIF2α in MiaPaCa-2 cells.

**B,** the effects of 72 hour CLS (50 uM or 25 uM) on PDAC cell death, as determined by PI staining and flow cytometry.

**C,** the effects of 72 hour CLS (50 uM or 25 uM) on lipid peroxidation in PDAC cells, as determined by C11-BODIPY staining and flow cytometry.

**D,** the effects of DFO (100 uM) and ferrostatin-1 (1 uM) treatment on cell death in PDAC cells after 72-hour CLS (25 uM) treatment.

**E and F,** the effects CLS (25 or 50 uM) on colony formation in naïve PDAC cells (E) or CLSA PDAC cells (F).

**G,** The effects of CLSA on cell proliferation in Capan-2 and SW1990 cells.

**H,** The effects of glutamine limitation (400 uM), arginine limitation (2 uM) and tryptophan limitation (10 uM) on colony formation (2 weeks) in MiaPaCa-2 cells.

**I,** The effects of glutamine limitation (400 uM) and BSA supplementation (5%) on MiaPaCa-2 colony formation (2 weeks).

**J,** MiaPaCa-2 cells were cultured in conventional DMEM media or Glu-limited DMEM (0.4 mM Glu plus 5% BSA) or Trp-limited DMEM (10 uM Trp) for 4 weeks before being used for cell proliferation assay in their respective nutrient replete or nutrient-limited cell culture media.

Data in (B-D) were analyzed using two sample, two-tailed paired Student's t-test. *** and **** represents p<0.001 and 0.0001, respectively.

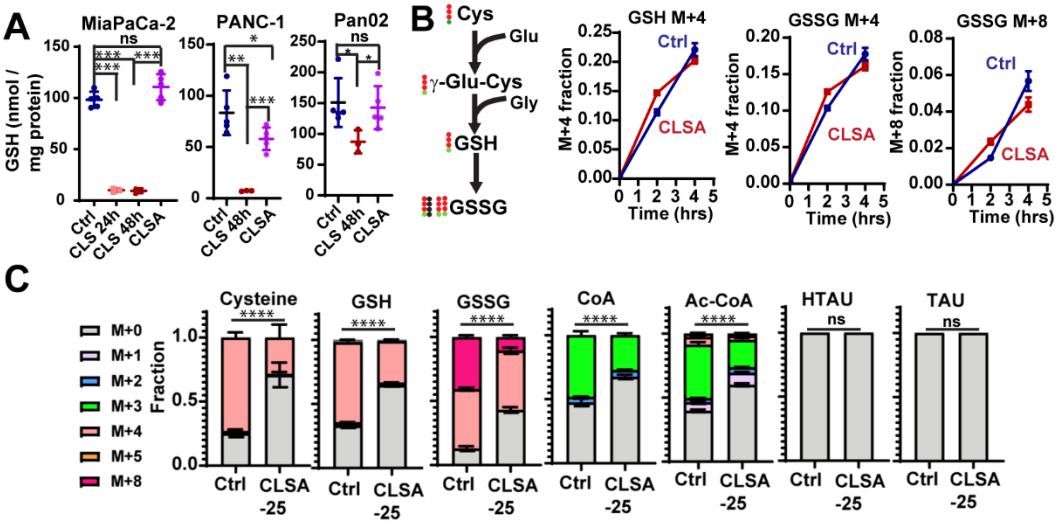


**Supplementary Figure 2. Cys metabolism in CLSA PDAC cells**

**A,** GSH levels in PDAC cells after being cultured in $Cys_2$-limited (25 uM) media for 24-48 hours, or after adaptation to 25 uM $Cys_2$-limitation for 4 weeks.

**B,** fractional labeling of M+4 GSH and M+4 or M+8 GSSG in control and CLSA-25 MiaPaCa-2 cells after incubation with [$^{13}C_6$, $^{15}N_2$]-$Cys_2$ for 2 or 4 hours.

**C,** steady state labeling of Cys metabolites after incubation with [$^{13}C_6$, $^{15}N_2$]-$Cys_2$ for 24 hours.

Data in (A and C) were analyzed using two sample, two-tailed paired Student's t-test. *** and **** represents p<0.001 and 0.0001, respectively. ns, not significant.

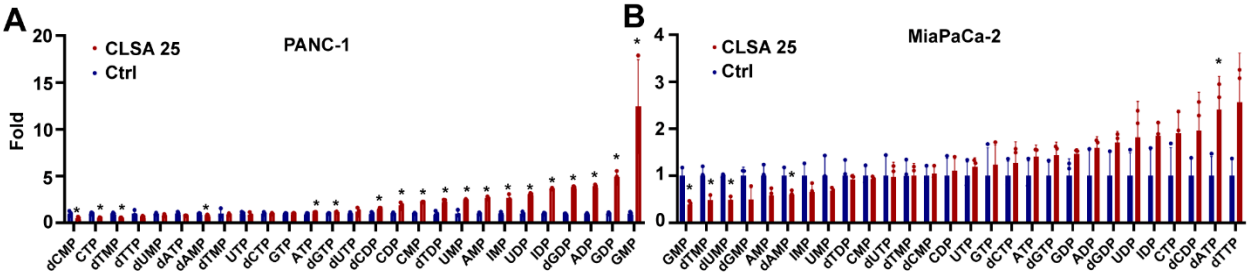


**Supplementary Figure 3. Elevated nucleotide levels in CLSA PDAC cells.**

**A and B**, bar graph showing the nucleotide levels in metabolomics screening using control or CLSA-25 PANC-1 (A) or MiaPaCa-2 (B) cells.

Data in (A-B) were analyzed using two sample, two-tailed paired Student's t-test. * indicates $p<0.05$.

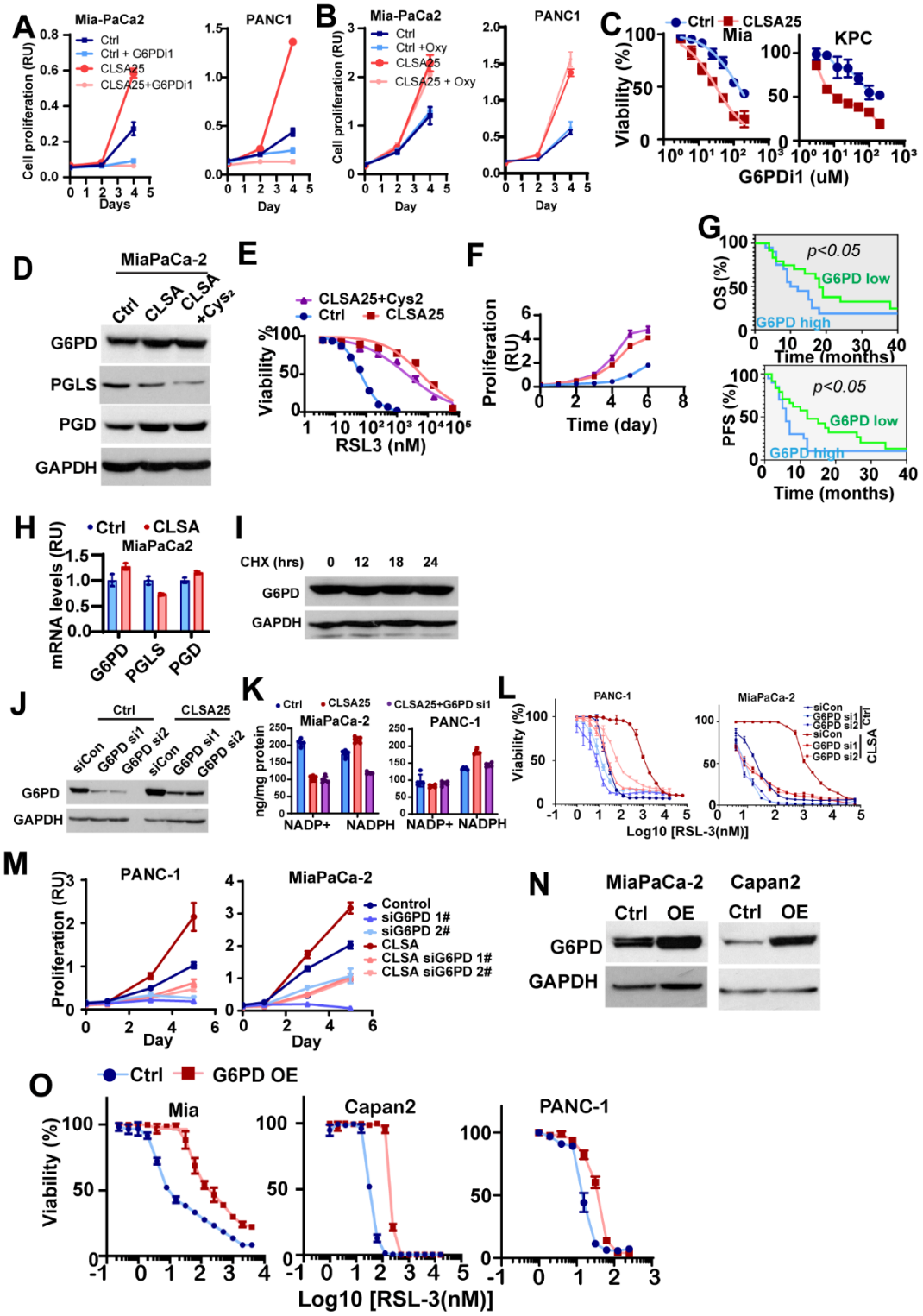


**Supplementary Figure 4. OxPPP is required for CLSA-mediated cell proliferation and ferroptosis resistance**

**A and B**, the effects of OxPPP inhibitor G6PDi1 (50 uM) and reductive PPP inhibitor oxythiamine (50 uM) treatment on cell proliferation in control or CLSA-25 PANC1 and MiaPaCa-2 cells.

**C,** the effect of G6PDi1 treatment on cell viability in control or CLSA-25 MiaPaCa-2 and KPC cells.

**D-F,** CLSA MiaPaCa2 cells retained its G6PD/PGD upregulation (**D**), ferroptosis resistance (E) and elevated cell proliferation (**F**) after being cultured in Cys2 replete medium for 1 month (CLSA+$Cys_2$).

**G,** mRNA transcript levels of G6PD, PGLS and PGD in control and CLSA-25 MiaPaCa-2 cells. **H,** inhibition of global translation with cycloheximide (100 ug/mL) had no effect on the protein expression levels of G6PD in MiaPaCa-2 cells.

**I,** correlation between G6PD staining intensity and overall survival (OS) and progression free survival (PFS) in a cohort of 100 PDAC patients.

**J,** effects of G6PD siRNA1 and 2 on the protein levels of G6PD in control or CLSA-25 MiaPaCa2 cells.

**K,** NADPH and NADP+ in MiaPaCa-2 and PANC1 cells used for the calculation of NADPH/NADP+ ratios in Fig. 4J.

**L,** the effects of G6PD knockdown on sensitivities to RSL-3 induced ferroptosis in control and CLSA-25 PDAC cells.

**M,** the effects of G6PD knockdown on cell proliferation in control and CLSA-25 PDAC cells.

**N,** G6PD expression levels in PDAC cells stably expressing pLX304 vector control or pLX304-G6PD.

**O,** the effects G6PD overexpression on RLS-3 induced ferroptosis sensitivities (L) or cell proliferation (M) in PDAC cells.

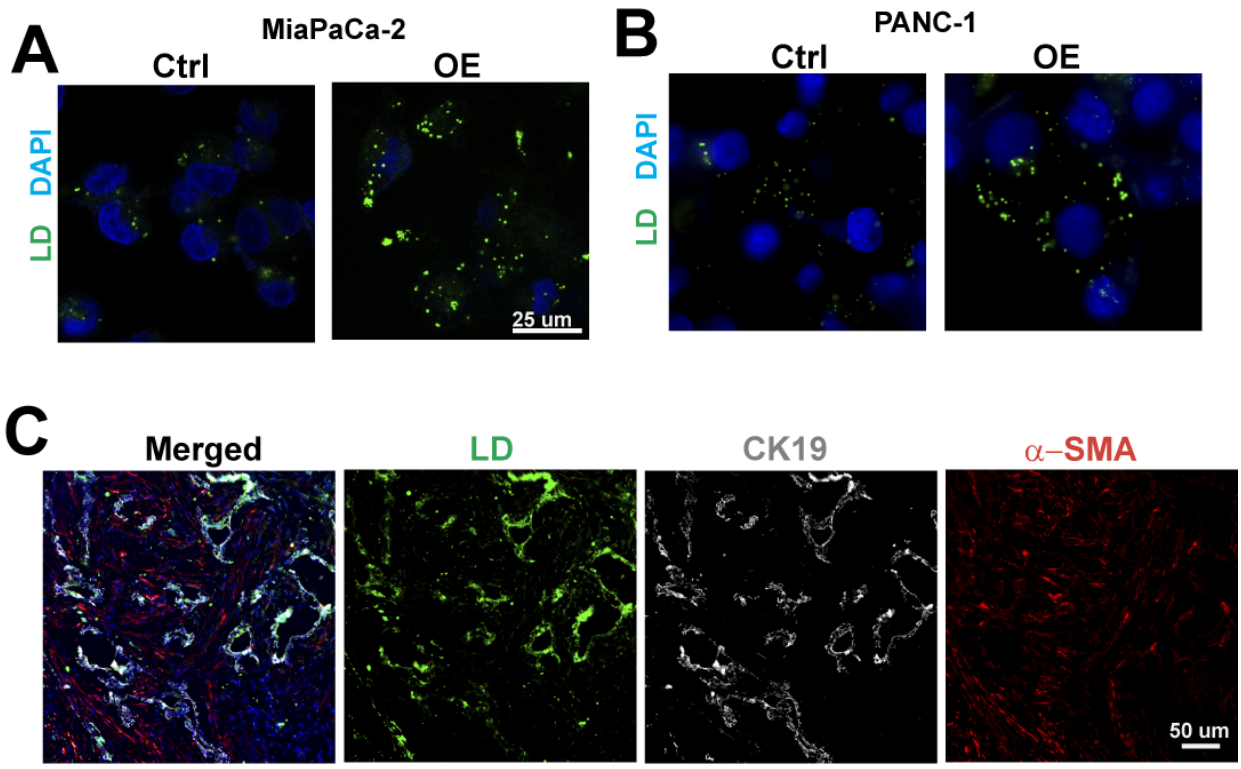


**Supplementary Figure 5. LD staining in PDAC cells and patient tissues.**

**A and B,** the effects of G6PD overexpression on LD levels in MiaPaCa-2 (A) and PANC-1 (B) cells.

**C,** LD staining in tumor cells (CK19) and cancer associated fibroblasts (α-SMA) in PDAC patient tissue sections.

**Table S1. Correlations between clinicopathological features and G6PD expression in pancreatic cancer**

**Table S1. Correlations between clinicopathological features and MCU expression in pancreatic cancer**

| | G6PD | | | |
|---|---|---|---|---|
| | Low | High | p-values | Spearman rank *r* value |
| **Gender** | | | | |

| | | | | |
|---|---|---|---|---|
| Male | 32 | 25 | 0.397 | 0.032 |
| Female | 18 | 25 | | |
| **Age** | | | | |
| > 60 | 27 | 28 | 0.755 | 0.086 |
| ≤60 | 23 | 22 | | |
| **Tumor size (cm)[b]** | | | | |
| ≤3 | 27 | 19 | 0.041 | 0.205 |
| >3 | 23 | 31 | | |
| **LN metastasis** | | | | |
| N 0 | 41 | 35 | <0.001 | 0.480 |
| N 1 | 9 | 15 | | |
| **pTNM stage** | | | | |
| I | 37 | 24 | **<0.001** | 0.376 |
| II, III | 13 | 26 | | |

## Reference


1. Schworer, S., Vardhana, S.A., and Thompson, C.B. (2019). Cancer Metabolism Drives a Stromal Regenerative Response. Cell Metab *29*, 576-591. 10.1016/j.cmet.2019.01.015.
2. Kamphorst, J.J., Nofal, M., Commisso, C., Hackett, S.R., Lu, W., Grabocka, E., Vander Heiden, M.G., Miller, G., Drebin, J.A., Bar-Sagi, D., et al. (2015). Human pancreatic cancer tumors are nutrient poor and tumor cells actively scavenge extracellular protein. Cancer Res *75*, 544-553. 10.1158/0008-5472.CAN-14-2211.
3. Badgley, M.A., Kremer, D.M., Maurer, H.C., DelGiorno, K.E., Lee, H.J., Purohit, V., Sagalovskiy, I.R., Ma, A., Kapilian, J., Firl, C.E.M., et al. (2020). Cysteine depletion induces pancreatic tumor ferroptosis in mice. Science *368*, 85-89. 10.1126/science.aaw9872.
4. Hirschhorn, T., and Stockwell, B.R. (2019). The development of the concept of ferroptosis. Free Radic Biol Med *133*, 130-143. 10.1016/j.freeradbiomed.2018.09.043.
5. Xie, Y., Zhu, S., Song, X., Sun, X., Fan, Y., Liu, J., Zhong, M., Yuan, H., Zhang, L., Billiar, T.R., et al. (2017). The Tumor Suppressor p53 Limits Ferroptosis by Blocking DPP4 Activity. Cell reports *20*, 1692-1704. 10.1016/j.celrep.2017.07.055.
6. Ward, N.P., and DeNicola, G.M. (2019). Sulfur metabolism and its contribution to malignancy. Int Rev Cell Mol Biol *347*, 39-103. 10.1016/bs.ircmb.2019.05.001.
7. Stockwell, B.R., Friedmann Angeli, J.P., Bayir, H., Bush, A.I., Conrad, M., Dixon, S.J., Fulda, S., Gascon, S., Hatzios, S.K., Kagan, V.E., et al. (2017). Ferroptosis: A Regulated

Cell Death Nexus Linking Metabolism, Redox Biology, and Disease. Cell *171*, 273-285. 10.1016/j.cell.2017.09.021.

8. Dixon, S.J., Lemberg, K.M., Lamprecht, M.R., Skouta, R., Zaitsev, E.M., Gleason, C.E., Patel, D.N., Bauer, A.J., Cantley, A.M., Yang, W.S., et al. (2012). Ferroptosis: an iron-dependent form of nonapoptotic cell death. Cell *149*, 1060-1072. 10.1016/j.cell.2012.03.042.
9. Yang, W.S., SriRamaratnam, R., Welsch, M.E., Shimada, K., Skouta, R., Viswanathan, V.S., Cheah, J.H., Clemons, P.A., Shamji, A.F., Clish, C.B., et al. (2014). Regulation of ferroptotic cancer cell death by GPX4. Cell *156*, 317-331. 10.1016/j.cell.2013.12.010.
10. Gaschler, M.M., and Stockwell, B.R. (2017). Lipid peroxidation in cell death. Biochem Biophys Res Commun *482*, 419-425. 10.1016/j.bbrc.2016.10.086.
11. Conrad, M., Kagan, V.E., Bayir, H., Pagnussat, G.C., Head, B., Traber, M.G., and Stockwell, B.R. (2018). Regulation of lipid peroxidation and ferroptosis in diverse species. Genes Dev *32*, 602-619. 10.1101/gad.314674.118.
12. Hassannia, B., Vandenabeele, P., and Vanden Berghe, T. (2019). Targeting Ferroptosis to Iron Out Cancer. Cancer Cell *35*, 830-849. 10.1016/j.ccell.2019.04.002.
13. Sullivan, M.R., Danai, L.V., Lewis, C.A., Chan, S.H., Gui, D.Y., Kunchok, T., Dennstedt, E.A., Vander Heiden, M.G., and Muir, A. (2019). Quantification of microenvironmental metabolites in murine cancers reveals determinants of tumor nutrient availability. Elife *8*. 10.7554/eLife.44235.
14. Commisso, C., Davidson, S.M., Soydaner-Azeloglu, R.G., Parker, S.J., Kamphorst, J.J., Hackett, S., Grabocka, E., Nofal, M., Drebin, J.A., Thompson, C.B., et al. (2013). Macropinocytosis of protein is an amino acid supply route in Ras-transformed cells. Nature *497*, 633-637. 10.1038/nature12138.
15. Vander Heiden, M.G., Cantley, L.C., and Thompson, C.B. (2009). Understanding the Warburg effect: the metabolic requirements of cell proliferation. Science *324*, 1029-1033. 10.1126/science.1160809.
16. Patra, K.C., and Hay, N. (2014). The pentose phosphate pathway and cancer. Trends in biochemical sciences *39*, 347-354. 10.1016/j.tibs.2014.06.005.
17. Lan, T., Arastu, S., Lam, J., Kim, H., Wang, W., Wang, S., Bhatt, V., Lopes, E.C., Hu, Z., Sun, M., et al. (2024). Glucose-6-phosphate dehydrogenase maintains redox homeostasis and biosynthesis in LKB1-deficient KRAS-driven lung cancer. Nature communications *15*, 5857. 10.1038/s41467-024-50157-8.
18. Li, Z., He, Y., Li, Y., Li, J., Zhao, H., Song, G., Miyagishi, M., Wu, S., and Kasim, V. (2021). NeuroD1 promotes tumor cell proliferation and tumorigenesis by directly activating the pentose phosphate pathway in colorectal carcinoma. Oncogene *40*, 6736-6747. 10.1038/s41388-021-02063-2.
19. Zhang, Y., Xu, Y., Lu, W., Li, J., Yu, S., Brown, E.J., Stanger, B.Z., Rabinowitz, J.D., and Yang, X. (2022). G6PD-mediated increase in de novo NADP. Sci Adv *8*, eabo0404. 10.1126/sciadv.abo0404.
20. Cheng, X., Geng, F., Pan, M., Wu, X., Zhong, Y., Wang, C., Tian, Z., Cheng, C., Zhang, R., Puduvalli, V., et al. (2020). Targeting DGAT1 Ameliorates Glioblastoma by Increasing Fat Catabolism and Oxidative Stress. Cell Metab *32*, 229-242 e228. 10.1016/j.cmet.2020.06.002.

21. Jarc, E., and Petan, T. (2019). Lipid Droplets and the Management of Cellular Stress. Yale J Biol Med *92*, 435-452.
22. Listenberger, L.L., Han, X., Lewis, S.E., Cases, S., Farese, R.V., Jr., Ory, D.S., and Schaffer, J.E. (2003). Triglyceride accumulation protects against fatty acid-induced lipotoxicity. Proc Natl Acad Sci U S A *100*, 3077-3082. 10.1073/pnas.0630588100.
23. Zadoorian, A., Du, X., and Yang, H. (2023). Lipid droplet biogenesis and functions in health and disease. Nat Rev Endocrinol *19*, 443-459. 10.1038/s41574-023-00845-0.
24. Shyu, P., Jr., Wong, X.F.A., Crasta, K., and Thibault, G. (2018). Dropping in on lipid droplets: insights into cellular stress and cancer. Biosci Rep *38*. 10.1042/BSR20180764.
25. Corbet, C., Bastien, E., Santiago de Jesus, J.P., Dierge, E., Martherus, R., Vander Linden, C., Doix, B., Degavre, C., Guilbaud, C., Petit, L., et al. (2020). TGFbeta2-induced formation of lipid droplets supports acidosis-driven EMT and the metastatic spreading of cancer cells. Nature communications *11*, 454. 10.1038/s41467-019-14262-3.
26. Senkal, C.E., Salama, M.F., Snider, A.J., Allopenna, J.J., Rana, N.A., Koller, A., Hannun, Y.A., and Obeid, L.M. (2017). Ceramide Is Metabolized to Acylceramide and Stored in Lipid Droplets. Cell Metab *25*, 686-697. 10.1016/j.cmet.2017.02.010.
27. Cotte, A.K., Aires, V., Fredon, M., Limagne, E., Derangere, V., Thibaudin, M., Humblin, E., Scagliarini, A., de Barros, J.P., Hillon, P., et al. (2018). Lysophosphatidylcholine acyltransferase 2-mediated lipid droplet production supports colorectal cancer chemoresistance. Nature communications *9*, 322. 10.1038/s41467-017-02732-5.
28. Rozeveld, C.N., Johnson, K.M., Zhang, L., and Razidlo, G.L. (2020). KRAS Controls Pancreatic Cancer Cell Lipid Metabolism and Invasive Potential through the Lipase HSL. Cancer Res *80*, 4932-4945. 10.1158/0008-5472.CAN-20-1255.
29. Brigham, M.P., Stein, W.H., and Moore, S. (1960). The Concentrations of Cysteine and Cystine in Human Blood Plasma. J Clin Invest *39*, 1633-1638. 10.1172/JCI104186.
30. Wang, X., Li, Y., Li, Z., Lin, S., Wang, H., Sun, J., Lan, C., Wu, L., Sun, D., Huang, C., et al. (2022). Mitochondrial Calcium Uniporter Drives Metastasis and Confers a Targetable Cystine Dependency in Pancreatic Cancer. Cancer Res *82*, 2254-2268. 10.1158/0008-5472.CAN-21-3230.
31. Apiz Saab, J.J., Dzierozynski, L.N., Jonker, P.B., AminiTabrizi, R., Shah, H., Menjivar, R.E., Scott, A.J., Nwosu, Z.C., Zhu, Z., Chen, R.N., et al. (2023). Pancreatic tumors exhibit myeloid-driven amino acid stress and upregulate arginine biosynthesis. Elife *12*. 10.7554/eLife.81289.
32. Zhu, J., Berisa, M., Schworer, S., Qin, W., Cross, J.R., and Thompson, C.B. (2019). Transsulfuration Activity Can Support Cell Growth upon Extracellular Cysteine Limitation. Cell Metab *30*, 865-876 e865. 10.1016/j.cmet.2019.09.009.
33. Lill, R., and Freibert, S.A. (2020). Mechanisms of Mitochondrial Iron-Sulfur Protein Biogenesis. Annual review of biochemistry *89*, 471-499. 10.1146/annurev-biochem-013118-111540.
34. Shukla, S.K., Purohit, V., Mehla, K., Gunda, V., Chaika, N.V., Vernucci, E., King, R.J., Abrego, J., Goode, G.D., Dasgupta, A., et al. (2017). MUC1 and HIF-1alpha Signaling

Crosstalk Induces Anabolic Glucose Metabolism to Impart Gemcitabine Resistance to Pancreatic Cancer. Cancer Cell *32*, 71-87 e77. 10.1016/j.ccell.2017.06.004.

35. Landgraf, P., Antileo, E.R., Schuman, E.M., and Dieterich, D.C. (2015). BONCAT: metabolic labeling, click chemistry, and affinity purification of newly synthesized proteomes. Methods Mol Biol *1266*, 199-215. 10.1007/978-1-4939-2272-7_14.
36. Park, J., Rho, H.K., Kim, K.H., Choe, S.S., Lee, Y.S., and Kim, J.B. (2005). Overexpression of glucose-6-phosphate dehydrogenase is associated with lipid dysregulation and insulin resistance in obesity. Molecular and cellular biology *25*, 5146-5157. 10.1128/MCB.25.12.5146-5157.2005.
37. Tsai, P.Y., Lee, M.S., Jadhav, U., Naqvi, I., Madha, S., Adler, A., Mistry, M., Naumenko, S., Lewis, C.A., Hitchcock, D.S., et al. (2021). Adaptation of pancreatic cancer cells to nutrient deprivation is reversible and requires glutamine synthetase stabilization by mTORC1. Proc Natl Acad Sci U S A *118*. 10.1073/pnas.2003014118.
38. Yang, S., Zhang, J.J., and Huang, X.Y. (2012). Mouse models for tumor metastasis. Methods Mol Biol *928*, 221-228. 10.1007/978-1-62703-008-3_17.
39. Liu, J., Bai, W., Zhou, T., Xie, Y., Yang, B., Sun, J., Wang, Y., Li, X., Hou, X., Liu, Z., et al. (2023). SDCBP promotes pancreatic cancer progression by preventing YAP1 from beta-TrCP-mediated proteasomal degradation. Gut *72*, 1722-1737. 10.1136/gutjnl-2022-327492.
40. Lin, S., Huang, C., Sun, J., Bollt, O., Wang, X., Martine, E., Kang, J., Taylor, M.D., Fang, B., Singh, P.K., et al. (2019). The mitochondrial deoxyguanosine kinase is required for cancer cell stemness in lung adenocarcinoma. EMBO molecular medicine *11*, e10849. 10.15252/emmm.201910849.
41. Sun, J., Lu, F., He, H., Shen, J., Messina, J., Mathew, R., Wang, D., Sarnaik, A.A., Chang, W.C., Kim, M., et al. (2014). STIM1- and Orai1-mediated Ca2+ oscillation orchestrates invadopodium formation and melanoma invasion. J Cell Biol *207*, 535-548. 10.1083/jcb.201407082.
42. Lin, S., Huang, C., Gunda, V., Sun, J., Chellappan, S.P., Li, Z., Izumi, V., Fang, B., Koomen, J., Singh, P.K., et al. (2019). Fascin Controls Metastatic Colonization and Mitochondrial Oxidative Phosphorylation by Remodeling Mitochondrial Actin Filaments. Cell reports *28*, 2824-2836 e2828. 10.1016/j.celrep.2019.08.011.
43. Kang, Y.P., Torrente, L., Falzone, A., Elkins, C.M., Liu, M., Asara, J.M., Dibble, C.C., and DeNicola, G.M. (2019). Cysteine dioxygenase 1 is a metabolic liability for non-small cell lung cancer. Elife *8*. 10.7554/eLife.45572.
44. Lin S., Li Y., Wang D., Huang C., Marino D., Bollt O., Wu C., Taylor M., Li W., DeNicola G. M., et al. (2021). The Actin Bundling Protein Fascin Promotes Lung Cancer Growth and Metastasis by Enhancing Glycolysis and PFKFB3 Expression. BioRxiv. https://doi.org/10.1101/2021.04.02.437070.